Article

Cell Reports

FOXO/DAF-16 Activation Slows Down Turnover of the Majority of Proteins in *C. elegans*

Graphical Abstract

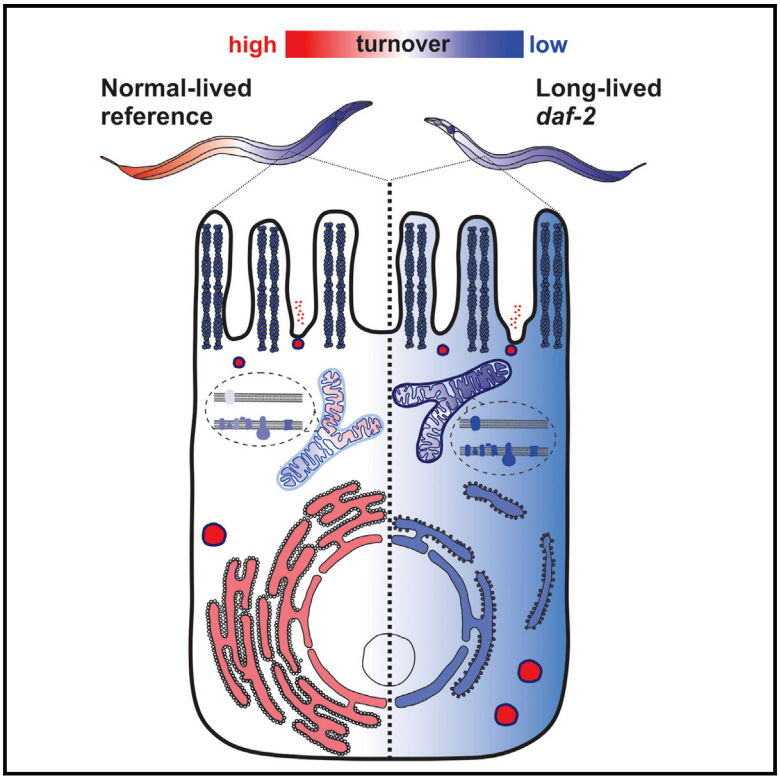

Authors

Ineke Dhondt, Vladislav A. Petyuk, Huaihan Cai, ..., Richard D. Smith, Geert Depuydt, Bart P. Braeckman

Correspondence

bart.braeckman@ugent.be

In Brief

Dhondt et al. apply a stable isotope labeling by nitrogen in *Caenorhabditis elegans* (SILeNCe) approach to unravel individual protein turnover dynamics in the long-lived insulin/insulin-like growth factor (IGF-1) receptor mutant *daf-2*.

Highlights

- Approximately 56% of the *daf-2* proteome showed decreased turnover
- This decrease was most prominent for components of the translation machinery
- Functional and spatial groups of proteins show distinct turnover patterns
- High protein turnover is not essential to support lifespan extension in *daf-2*

Dhondt et al., 2016, Cell Reports *16*, 3028–3040
September 13, 2016 © 2016 The Author(s).
http://dx.doi.org/10.1016/j.celrep.2016.07.088

OPEN ACCESS
CellPress

Cell Reports
Article

FOXO/DAF-16 Activation Slows Down Turnover of the Majority of Proteins in *C. elegans*

Ineke Dhondt,[1,4] Vladislav A. Petyuk,[2,4] Huaihan Cai,[1] Lieselot Vandemeulebroucke,[1] Andy Vierstraete,[1] Richard D. Smith,[2] Geert Depuydt,[1,3] and Bart P. Braeckman[1,5,*]

[1]Laboratory for Aging Physiology and Molecular Evolution, Biology Department, Ghent University, Proeftuinstraat 86 N1, 9000 Ghent, Belgium
[2]Biological Sciences Division, Pacific Northwest National Laboratory, Richland, WA 99352, USA
[3]Laboratory for Functional Genomics and Proteomics, Department of Biology, KU Leuven, Naamsestraat 59, 3000 Leuven, Belgium
[4]Co-first author
[5]Lead Contact
*Correspondence: bart.braeckman@ugent.be
http://dx.doi.org/10.1016/j.celrep.2016.07.088

SUMMARY

Most aging hypotheses assume the accumulation of damage, resulting in gradual physiological decline and, ultimately, death. Avoiding protein damage accumulation by enhanced turnover should slow down the aging process and extend the lifespan. However, lowering translational efficiency extends rather than shortens the lifespan in *C. elegans*. We studied turnover of individual proteins in the long-lived *daf-2* mutant by combining SILeNCe (stable isotope labeling by nitrogen in *Caenorhabditis elegans*) and mass spectrometry. Intriguingly, the majority of proteins displayed prolonged half-lives in *daf-2*, whereas others remained unchanged, signifying that longevity is not supported by high protein turnover. This slowdown was most prominent for translation-related and mitochondrial proteins. In contrast, the high turnover of lysosomal hydrolases and very low turnover of cytoskeletal proteins remained largely unchanged. The slowdown of protein dynamics and decreased abundance of the translational machinery may point to the importance of anabolic attenuation in lifespan extension, as suggested by the hyperfunction theory.

INTRODUCTION

Cellular protein quality can be maintained by proteolytic elimination of damaged proteins and replacing them with newly synthesized copies, a process called protein turnover (Ward, 2000). Protein turnover rates have been estimated using SILAC (stable isotope labeling by amino acids in cell culture) in prokaryotes and eukaryotes. The last decade has witnessed a growing interest in the analysis of whole-organism proteome dynamics in metazoans using the same approach (Claydon and Beynon, 2012). In recent work, SILAC was applied to monitor protein synthesis throughout life in adult *Caenorhabditis elegans* (Vukoti et al., 2015) and to investigate food intake (Gomez-Amaro et al., 2015).

Progressive decrease in protein synthesis and proteolytic clearance through the autophagosomal and proteasome systems with age results in a strong increase in protein half-life in many species, including nematodes (Grune, 2000; Lewis et al., 1985; Young et al., 1975). This finding led to the formulation of the protein turnover hypothesis, stating that the increase in protein dwell time with age results in the accumulation of damaged and misfolded proteins. The progressive decrease in general protein turnover might be responsible for the ultimate collapse of proteome homeostasis in aging cells, possibly also driving the aging process itself (Rattan, 1996; Ryazanov and Nefsky, 2002; Taylor and Dillin, 2011). In this vein, it is expected that increased protein turnover rates would help to maintain a young undamaged proteome and extend the lifespan. However, in yeast and *C. elegans,* genetically induced attenuation of protein synthesis extends, rather than shortens, the lifespan (Hansen et al., 2007; Kaeberlein et al., 2005; Pan et al., 2007; Syntichaki et al., 2007). Moreover, classical ^{35}S pulse-chase labeling and quantitative proteomic studies suggest that low overall protein synthesis is a hallmark of long-lived *C. elegans*, either by dietary restriction or by mutation in the insulin signaling pathway (Depuydt et al., 2013, 2016; Stout et al., 2013). Similar findings have been reported for diet-restricted mice (Price et al., 2012). Hence, why does reducing protein synthesis promotes lifespan extension? And how can this be reconciled with the protein turnover hypothesis, which predicts enhanced turnover rates in long-lived organisms?

The DAF-16 homologue Forkhead box O (FOXO)/DAF-16 transcription factor drives the increased longevity of the insulin/insulin-like growth factor (IGF-1) receptor mutant *daf-2* (Kenyon et al., 1993). We hypothesized that DAF-16-dependent longevity in *C. elegans* is supported by differential protein turnover. Down-regulating turnover of the majority of proteins could save much energy, which, in turn, could be spent at prioritized maintenance of specific proteins that are crucial to extend the lifespan. To test this hypothesis, we used stable isotope labeling by nitrogen in *Caenorhabditis elegans* (which we now designate SILeNCe), an efficient method applied in *C. elegans* before (Geillinger et al., 2012; Krijgsveld et al., 2003). Here we present a SILeNCe

This is an open access article under the CC BY-NC-ND license (http://creativecommons.org/licenses/by-nc-nd/4.0/).

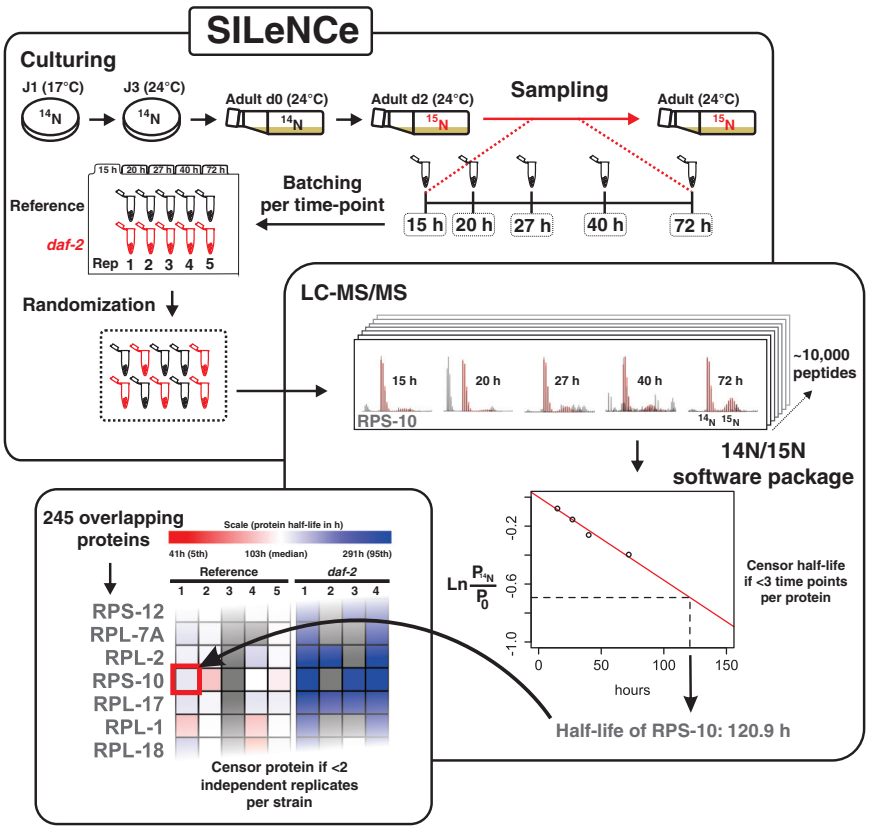

Figure 1. Study Design

A ^{15}N metabolic labeling approach was performed to study individual protein turnover rates in long-lived *daf-2 C. elegans*. Adult worms were sampled at regular time points after pulsing with ^{15}N-labeled *E. coli*. Samples were blocked based on the time of the pulse, randomized, and blindly analyzed using LC-MS/MS. The resulting datasets were processed using a custom R package. Protein half-lives of 245 overlapping proteins between reference and *daf-2* worms were estimated for five and four biological replicates, respectively.

dataset that reveals patterns of intracellular protein dynamics in the *C. elegans* model and shifts of these patterns that occur in the long-lived *daf-2* mutant via DAF-16 activation.

RESULTS

Worm Strains Used to Study Protein Turnover in Long-Lived *daf-2*

To understand the role of protein turnover in DAF-16-mediated lifespan extension, we chose to compare the normal-lived *glp-4(bn2) daf-16(mgDf50); daf-2(e1370)* triple mutant (reference strain) and the long-lived *glp-4(bn2); daf-2(e1370)* insulin/IGF-1 receptor mutant. Mutation in DAF-2 causes activation of the downstream transcription factor DAF-16, which, in turn, activates a life maintenance program, doubling the lifespan of *C. elegans*. To specifically study DAF-16, the major lifespan regulator, we compared two worm strains carrying the *daf-2* mutation (causing lifespan extension via DAF-16 activation) and knocked out the *daf-16* gene by mutation in the reference strain, thereby nullifying the lifespan extension phenotype. The use of a temperature-sensitive sterile mutant background (*glp-4*) enables us to focus on somatic cells and avoids purging of the ^{15}N label via egg laying. The *glp-4* mutation has only minimal effects on the lifespan of wild-type and *daf-16* nematodes (TeKippe and Aballay, 2010). However, it acts as an enhancer of *daf-2* longevity (McColl et al., 2005; McElwee et al., 2004), probably via surplus activation of DAF-16 (Arantes-Oliveira et al., 2002; Hsin and Kenyon, 1999; Lin et al., 2001), which makes it an even better strain to study the DAF-16 effect on lifespan. Mass spectrometry (MS) proteome profiling of *glp-4(bn2)* revealed only modest changes relative to the N2 wild-type (Krijgsveld et al., 2003). Recently, it was found that *glp-4* encodes a valyl aminoacyl tRNA synthetase, suggesting reduced protein translation in the mutant (Rastogi et al., 2015). We verified this prediction with classical ^{35}S pulse-chase labeling and did not observe a difference in protein synthesis and degradation rates between the *glp-4* mutant and other control strains, including wild-type N2 (Figure S1). The strategy of comparing *glp-4; daf-2* with *glp-4 daf-16;daf-2* has been used earlier by others (Depuydt et al., 2013, 2014; McElwee et al., 2007). Lifespan curves of these strains cultured under identical conditions as in this study have been published earlier (Depuydt et al., 2013). For clarity and simplicity, these strains will be designated as reference (*glp-4(bn2) daf-16(mgDf50); daf-2(e1370)*) and *daf-2* (*glp-4(bn2); daf-2(e1370)*) for the remainder of this article.

DAF-16 Activation Increases Global Proteomic Half-Life

In the SILeNCe experiment, worms were fed ^{15}N-labeled *E. coli* bacteria on the second day of adulthood, avoiding possible changes in relative protein composition related to development. From this moment, samples were taken at regular time points. Accurate MS-based quantitative proteomics were performed in a randomized and blind manner (Table S3). The resulting 43 MS datasets were analyzed using a custom R package to extract the proportions of heavy (^{15}N) and light (^{14}N) isotope peaks of the peptides, followed by estimation of the corresponding protein half-lives (Figure 1). Data were statistically evaluated using the moderated t test from the *limma* R package (Ritchie et al., 2015). The use of a conservative pipeline enabled us to generate a very solid dataset with the tradeoff of reduced protein diversity (Figure S2A). However, the proteins covered in our experiment make up 30.8% of total worm mass, as estimated from integrated proteomic *C. elegans* studies (Figure S2B; Wang et al., 2015). We observed significantly decreased peptide turnover rates for 185 (i.e., 54%) of the analyzed peptides in *daf-2* compared with the reference strain ($p < 0.05$). Only five peptides exhibited

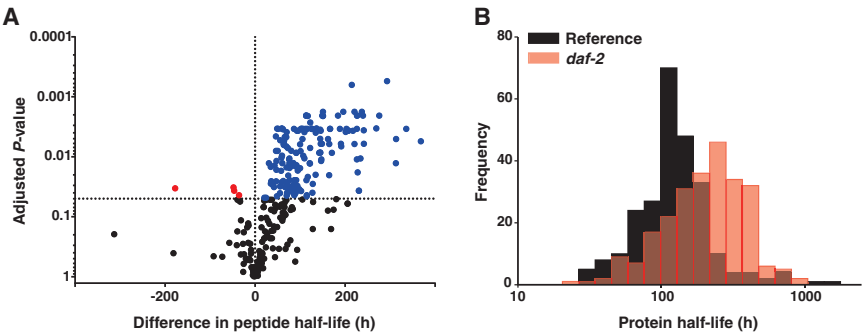

Figure 2. Slowdown of Protein Turnover in *daf-2*

(A) Volcano plot representing peptides with upregulated (red dots), downregulated (blue dots), and unchanged (black dots) turnover and their corresponding change in peptide half-life in *daf-2*. p Values were obtained from the moderated t test implemented in the *limma* R package and adjusted for multiple testing according to Benjamini and Hochberg's method.

(B) Histogram showing the distribution of protein half-lives for reference and *daf-2* worms. The median protein half-life is 103 hr for the reference strain and 173 hr for *daf-2*.

Source data are available in Table S1.

significantly faster replacement rates in *daf-2*, and turnover of 155 (i.e., 45%) peptides was unaltered (Figure 2A). This observation was confirmed with a classical ^{35}S pulse-chase experiment showing overall reduced protein synthesis and degradation rates in *daf-2* compared with the reference. Although this downtrend is somewhat less pronounced in the *glp-4* genetic background, the global tendency is preserved. Moreover, loss of *daf-16* in the *daf-2* mutant background reverts protein turnover back to reference levels (Figure S1). The half-lives of redundant peptides from each protein were averaged. In total, we compared 245 overlapping non-redundant proteins from the reference and *daf-2* (Table S1). Turnover rates vary widely, with half-lives ranging from 40 hr to more than 40 days. Mutation in *daf-2* leads to a shift in median protein half-life from 103 hr to 173 hr (Figure 2B). According to the protein turnover hypothesis, the longer protein half-life in *daf-2* should lead to increased damage accumulation. Hence, we specifically screened the liquid chromatography-tandem mass spectrometry (LC-MS/MS) datasets (0 hr time point) for signatures of protein damage via spectral counting. We observed a significantly lower level (~32%) of methionine oxidation in long-lived *daf-2* (Poisson-based generalized linear model, $p < 0.001$; Figure S3), which parallels earlier carbonylation data (Yang et al., 2007). This may be explained by the elevated expression of antioxidants (Honda and Honda, 1999) and high reductive capacity (Houthoofd et al., 2005) in *daf-2* mutants. Other common types of protein damage, such as non-tryptic protein degradation and deamidation, do not differ between young *daf-2* and reference worms. Our data show that decreased protein turnover rate does not necessarily correlate to increased accumulation of protein damage. Although it is still unclear to what extent low oxidative damage levels influence the downregulation of protein turnover in *daf-2*, this process is likely actively regulated as described by Essers et al. (2015).

Changes in Protein Half-Life Do Not Correlate with Changes in Abundance

We compared the relative changes in protein turnover with relative protein abundance shifts of the same strains published earlier by our group (Depuydt et al., 2013). Correlation analysis was performed on the 167 proteins in common between both datasets (Table S2). Overall, the relative changes in protein abundance because of mutation in *daf-2* do not correlate with those in protein turnover ($R^2 = 0.0054$, $p = 0.3447$ for the Pearson correlation; Figure 3). This lack of correlation indicates that the change in abundance of a particular protein is not necessarily dictated by its relative turnover. This is showcased in the fermentation enzymes SODH-1 and ALH-1: both proteins show a similar increase in protein half-lives, although disparate increases in mRNA expression (McElwee et al., 2007) and protein levels (Depuydt et al., 2013) have been observed (Figure 3, inset). Furthermore, a contrasting pattern is found between mitochondrial and ribosomal proteins. The relative mitochondrial protein abundance is increased, whereas turnover rates are decreased in *daf-2* mutants. Because mitochondrial proteins represent a large fraction of the total cellular protein, this decrease in mitochondrial turnover may represent a considerable energy saving in *daf-2*. The ribosomal proteins, another family of highly abundant proteins, follow the opposite pattern: both turnover and relative abundance are decreased in *daf-2* mutants (Figure 3). Here, energy saving may be combined with an actual functional reduction, as discussed below.

Turnover of the Protein Synthesis Machinery Is Slowed Down in *daf-2*

The half-life of proteins associated with the protein synthesis machinery is significantly increased in *daf-2* mutants. In reference animals, ribosomal proteins have half-lives of approximately 100 hr, whereas, in *daf-2* mutants, these figures are increased 2- to 4-fold. Proteins of the small (40S) and large (60S) ribosomal subunits show similar turnover rates, and a comparable increase in half-life was observed for both subunits in *daf-2* (Figures 4 and 5A). In addition, we found a similar pattern for translation factors, also involved in protein synthesis (Figure 5B). Endoplasmic reticulum (ER)-bound ribosomes synthesize proteins, which are translocated into the ER lumen, where they are subsequently folded and assembled with the aid of specialized proteins (Vázquez-Martínez et al., 2012). Interestingly, we found prolonged half-lives for all detected ER proteins predicted to be involved in these processes in the *daf-2* mutant (Figure 5C). The average protein half-life of ER proteins is only 86 hr in reference worms and shifts significantly toward 173 hr in *daf-2* mutants (two-sample Student's t test, $p < 0.0001$). In the same line, *daf-2* mutants show a loose pattern of rough ER (RER) cisternae dispersed through the cytoplasm, sparsely studded with ribosomes (Figure 6), whereas, in the reference strain, abundant RER is densely stacked in Terasaki ramps to accommodate maximum protein synthesis within the confined cells (Heald and Cohen-Fix, 2014; Terasaki et al., 2013). However,

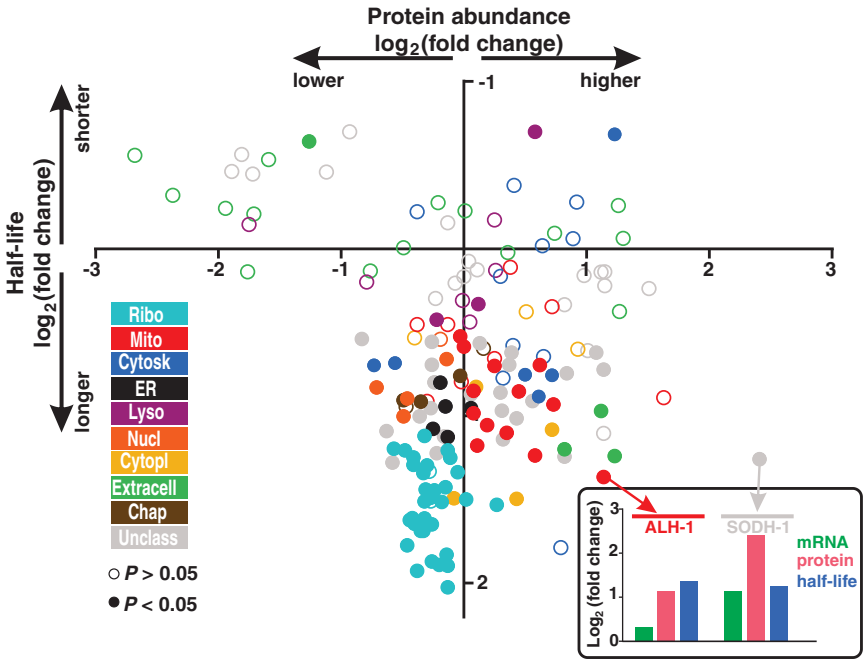

Figure 3. Changes in Protein Turnover and Abundance Do Not Correlate in *daf-2*

Scatterplot illustrating the fold change (log_2) of protein abundance and protein turnover in *daf-2* relative to the reference strain (origin). Significant changes in protein turnover ($p < 0.05$) are signified with closed circles. p values were obtained from the moderated t test implemented in the *limma* R package and adjusted for multiple testing according to Benjamini and Hochberg's method. Ribo, ribosomal; Mito, mitochondrial; Cytosk, cytoskeletal; ER; Lyso, lysosomal; Nucl, nuclear; Cytopl, cytoplasmic; Extracell, extracellular; Chap, chaperones; Unclass, unclassified proteins. Inset: case study of SODH-1 and ALH-1 demonstrating discordance between transcript (McElwee et al., 2007) and protein (Depuydt et al., 2013) abundance versus protein half-life (fold change [log_2]) in *daf-2*. Source data are available in Table S2.

despite the dispersed RER arrangement, decreased ribosomal load, and lower refreshment rates of ER-associated proteins, the half-lives of RER-processed proteins (secretory proteins and lysosomal proteins), remain unchanged in *daf-2* mutants (Figures 4A and 4B, insets).

Lysosomal Protein Turnover: High in the Lumen but Low in the Membrane

Autophagy is the major degradation pathway of macromolecules and organelles, and this process involves lysosome-mediated catabolism (Yorimitsu and Klionsky, 2005). We identified four lysosomal proteins whose turnover is very fast (average half-life, 38 hr) and similar in the reference strain and *daf-2* mutant, whereas the half-life of only one hydrolase, the cathepsin ASP-4 (1.6-fold down, $p = 0.0436$) is slightly altered (Figure 5J). Acidification of the lysosomal lumen depends on the activity of proton pumps, vacuolar-type H^+ ATPase complexes, present in the lysosomal membrane (Mindell, 2012). As opposed to the fast intraluminal hydrolase turnover, we found very slow replacement rates for subunits of the V1 cytosolic complex in both reference and *daf-2* worms (average half-life, 225 hr; Figure 5K). Only two subunits, VHA-8 and VHA-14, show a slight but significant reduction in protein half-lives in *daf-2* ($p = 0.0328$ and $p = 0.0319$, respectively). Unexpectedly, the turnover rate of VHA-11, the subunit C homolog of the V1 complex, is very fast in reference worms (50 hr, one replicate) and exceptionally high in *daf-2* worms (average half-life, 9 hr; three biological replicates). In general, however, we observed significantly longer protein half-lives for membrane-associated proteins compared with intraluminal proteins for both reference and *daf-2* mutants (unpaired Student's t test, $p < 0.0001$ and $p = 0.00021$, respectively). A similar distinction between membrane-bound and free proteins was observed within mitochondria.

Mitochondrial Turnover Is Decreased in *daf-2*

Mitochondrial proteins may be vulnerable to oxidative damage because of their proximity to reactive oxygen species (ROS)-generating centers (Murphy, 2009). Therefore, it could be expected that mitochondrial proteins exhibit high refreshment rates to maintain their important vital function. Contrary to prediction, 65% of the identified mitochondrial proteins exhibit longer half-lives in *daf-2* compared with the reference strain ($p < 0.05$), whereas the remaining proteins do not show any significant change. To corroborate this finding, we expressed Dendra2 in the mitochondria of all cells (Figure 5D). We measured the red Dendra2 fluorescence intensity of transgene worms at different time points after photoconversion for the reference and *daf-2* worms and monitored the decrease of the relative red signal over time as a proxy of mitochondrial protein breakdown. Consistent with our SILeNCe data, the decrease of the red fluorescence is slowed down significantly in *daf-2* mutants compared with the reference strain (F-test, $p < 0.0001$; Figure 5I). With this method, we estimated the half-life of the mitochondrially targeted Dendra2 protein to be 44 hr in the reference strain and 77 hr in *daf-2* mutants. Interestingly, the turnover of Dendra2 is comparable with the fastest turnover rates observed for mitochondrial matrix-resident proteins (Figure 5E). This high turnover might be due to the fact that Dendra2 is a foreign protein and, therefore, probably more likely to be degraded by mitochondrial proteases. As in lysosomes, turnover of membrane-bound mitochondrial proteins is significantly slower compared with the turnover of free proteins for both strains studied, although this difference is less prominent in *daf-2* mutants (Figures 4C and 4D; two-sample Student's t test, $p < 0.0001$ and $p = 0.0096$, respectively). Widely divergent protein half-lives were found for mitochondrial matrix proteins, ranging from 52–183 hr in the reference strain and 103–358 hr in *daf-2* mutants (Figure 5E). In addition, mitochondrial protein turnover shows limited uniformity within biochemical pathways in reference worms. For instance, the citric acid cycle enzymes

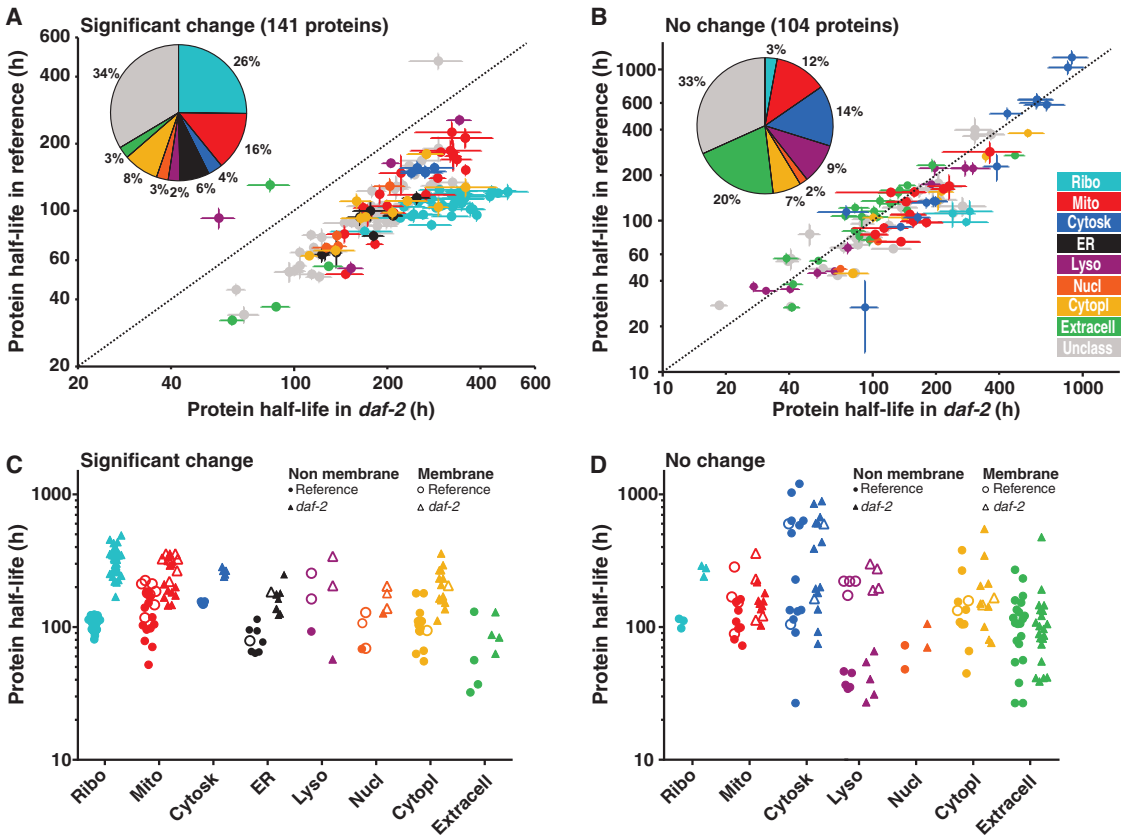

Figure 4. Protein Dynamics in Subcellular Compartments

(A and B) Scatterplot comparing significant (A) and non-significant (B) changes of protein half-lives in *daf-2* versus the reference strain. Functional groups are color-coded and summarized in pie chart insets. p Values were obtained from the moderated t test implemented in the *limma* R package and adjusted for multiple testing according to Benjamini and Hochberg's method. Error bars are SEM.

(C and D) Protein half-lives in different cellular compartments with differentiation of membrane-bound proteins (open symbols) and free proteins (filled symbols). Significantly changed half-lives are represented in (C) (two-sample Student's t test, $p < 0.05$), and non-significant changes are depicted in (D).

Source data are available in Table S4.

fumarase (FUM-1) and malate dehydrogenase (MDH-1) show half-lives of 81 and 162 hr, respectively. Nevertheless, an overall reduction in protein half-life of the carbohydrate metabolic enzymes is observed in *daf-2* (Figure S4). On the other hand, proteins of the mitochondrial membrane, including subunits of the electron transport chain and adenine nucleotide transporters, display very slow turnover rates compared with most matrix proteins. This slow turnover is further decreased in *daf-2* for most proteins (Figures 5F–5H).

Minimal Turnover of Cytoskeletal and Muscle-Related Proteins

Proteins of the muscle contractile apparatus, such as thin filament actins and myosin class II light-chain proteins, exhibit extremely long protein half-lives (on average 25 and 41 days, respectively; Figure 5L). These numbers suggest that myofilaments only undergo occasional turnover during the entire *C. elegans* lifespan. We observed slow turnover for the isoform myosin class II heavy-chain protein UNC-54 (half-life on average 298 hr), but we did not detected any label incorporation at all for the other three isoforms, which suggests a complete lack of turnover. On the other hand, the invertebrate-specific paramyosin UNC-15, which interacts with these heavy-chain proteins, shows remarkably fast turnover in both reference and *daf-2* mutants (average half-life, 66 hr). Other proteins involved in muscle physiology show moderate protein half-lives in reference worms (140 hr on average) and are somewhat delayed in *daf-2* mutants without reaching significance (202 hr on average). Only the putative creatine kinase W10C8.5 and the triosephosphate isomerase TPI-1 have significantly reduced turnover rates in *daf-2* ($p = 0.0062$ and $p = 0.0293$, respectively). These proteins, involved in the supply of energy molecules in muscle cells (Ralser et al., 2007; Wallimann et al., 2011), show strong DAF-16-dependent upregulation (Depuydt et al., 2013). Increased protein levels in combination with lower rates of turnover suggest an upkeep of these proteins. Low turnover was also found for cytoskeletal proteins that reside in the cytoplasm. ACT-5, an intestine-specific actin, displays a long protein half-life analogous to muscle actins. The constituents of microtubules, alpha- and beta-tubulins, are less stable, with an average half-life around 141 hr in reference worms. Protein half-lives of beta-tubulins remain unchanged in *daf-2* (168 hr on average),

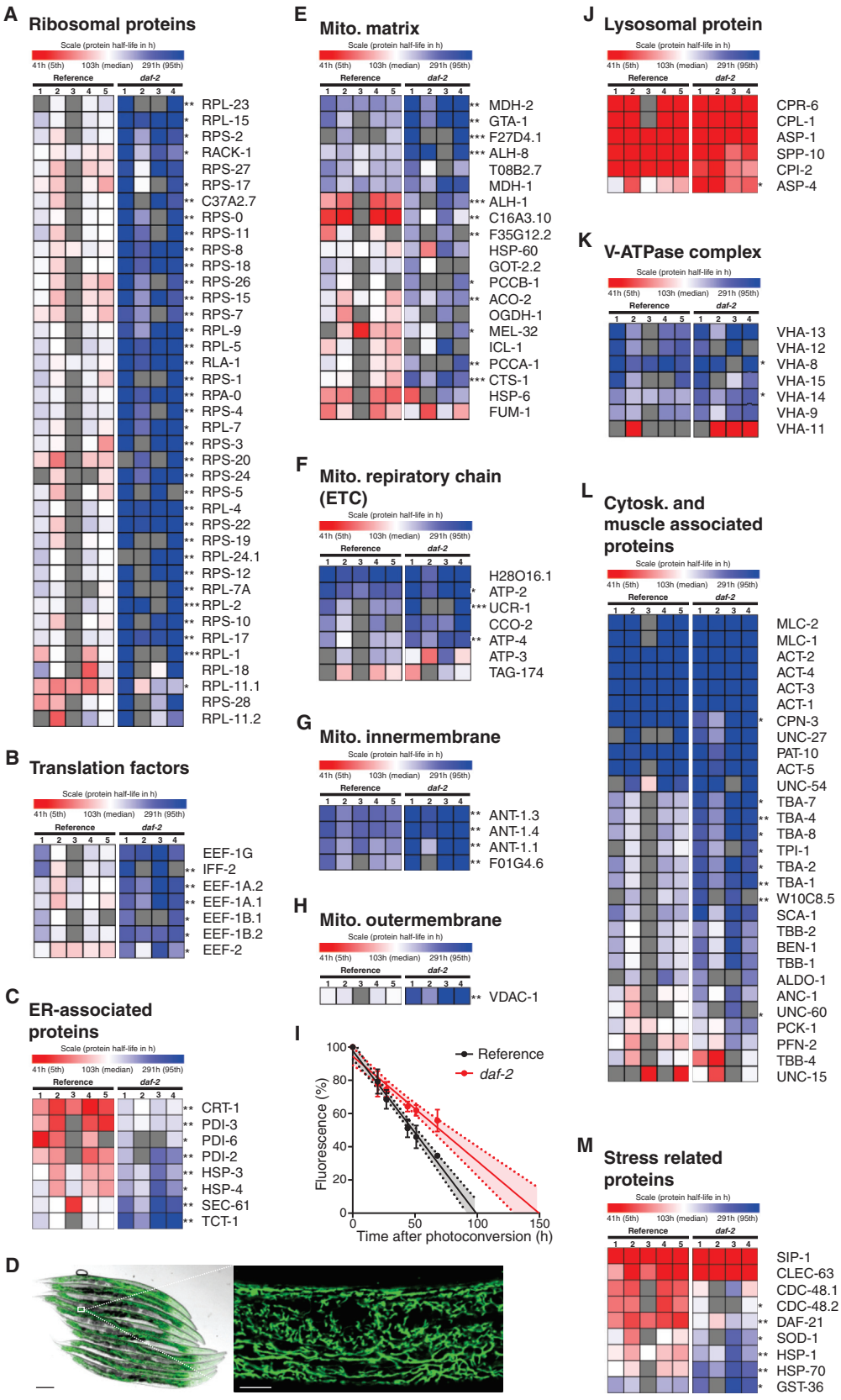

(legend on next page)

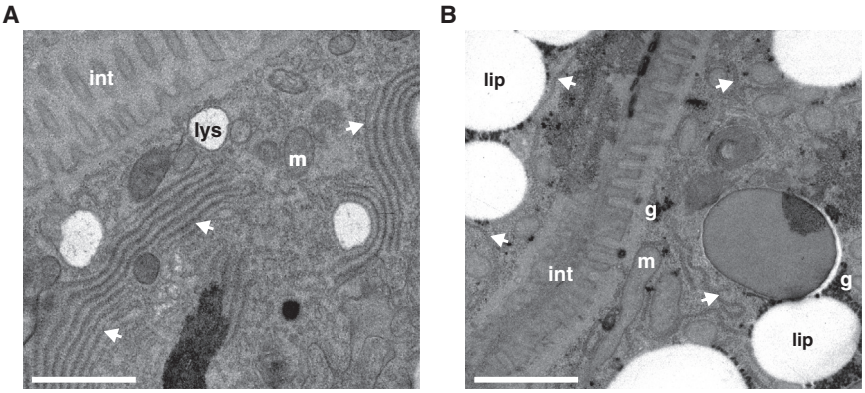

Figure 6. Organization of the Rough Endoplasmic Reticulum

(A and B) Transmission electron micrographs of intestinal cells of reference (A) and *daf-2* worms (B). Arrows indicate the RER. int, intestine; lys, lysosome; m, mitochondrion; g, glycogen; lip, lipid. Scale bars, 1 μm.

whereas turnover of alpha-tubulins is significantly attenuated (average half-life, 261 hr; $p < 0.05$).

Reduced Turnover of Stress Response Proteins in *daf-2*

Much evidence points to a strong correlation between longevity and cytoprotective mechanisms, linking lifespan extension to an increased tolerance to a variety of stressors (Shore et al., 2012). We observed a wide range of stress protein half-lives, ranging from 27–159 hr in the reference worms and 41–236 hr in *daf-2* mutants (Figure 5M). Stress-induced cytosolic chaperones, including heat shock proteins (HSPs), show fast to moderate turnover rates in the reference strain (average half-life, 68 hr). Surprisingly, these proteins show reduced turnover in long-lived *daf-2* mutants (average half-life, 132 hr), with a significant diminution for DAF-21, HSP-1, HSP-70, and CDC-48.2. These observations are in line with the extended protein half-lives for HSPs of the ER, as described above. Several HSPs are downregulated in *daf-2* (Depuydt et al., 2013), including DAF-21 and HSP-1, which implies that, contrary to expectation, *daf-2* worms invest less energy in the abundance and turnover of HSPs. In addition, other proteins involved in cytoprotection showed a similar pattern, including glutathione-S-transferase (GST) 36 (1.48-fold down, $p = 0.0107$), involved in xenobiotic detoxification (Ayyadevara et al., 2007), and superoxide dismutase (SOD) 1 (Figure 5M; 1.82-fold down, $p = 0.0144$). However, not all *daf-2* stress proteins show decreased turnover; e.g., turnover of SIP-1 (average half-life, 33 hr), a small heat shock protein, is unaffected in *daf-2* mutants. A similar pattern was observed for CLEC-63, an antimicrobial protein involved in the worms' innate immunity (average half-life, 49 hr). Our data suggest that, to some extent, *daf-2* saves energy by reducing the turnover of specific cytoprotective proteins.

Dendra2 Photoswitching Validates the SILeNCe Approach

As an alternative approach to SILeNCe, we constructed reporters expressing the green-to-red photoswitchable fluorescent protein Dendra2 from the octocoral *Dendronephthya* (Gurskaya et al., 2006). Green-to-red fluorescence photoconversion is an irreversible process. Hence, surveying the decrease of red Dendra2 fluorescence over time (protein degradation) is an alternative estimate of protein half-live that is insensitive to label uptake or re-use. To validate the slowdown of ribosomal turnover and the short lysosomal protein half-lives assessed with SILeNCe (Figure 7A), we expressed Dendra2 fused to the ribosomal RLA-1 protein and lysosomal ASP-4 hydrolase in long-lived *daf-2*, respectively. We monitored the change in red fluorescence intensity with confocal microscopy after 96 hr (for RLA-1) and 48 hr (for ASP-4) after photoconversion. We observed a prolonged protein half-life of RLA-1 in the long-lived *daf-2* compared with the reference worms fed with *daf-16* RNAi (two-sample Student's t test, $p = 0.0019$; Figures 7B and 7C), which confirms the reduced turnover of this ribosomal subunit upon DAF-16 activation (Figure 7A). Likewise, we corroborated the preserved fast protein turnover of ASP-4 via the Dendra2 method (two-sample Student's t test, $p = 0.6278$; Figures 7B and 7D). Hence, estimating protein turnover using Dendra2 photoconversion validated our observations from the SILeNCe method.

DISCUSSION

Proteins with long dwelling times are likely to accumulate all sorts of molecular damage during aging. Thus, one could expect that, by increasing the protein turnover rate, cellular damage accumulation is prevented and the lifespan is extended. However, several studies are in conflict with the turnover hypothesis, as they observe overall decreased protein synthesis rates in *C. elegans* longevity mutants, or, vice versa, translation inhibition results in lifespan extension (Depuydt et al., 2013; Hansen et al.,

Figure 5. Individual Protein Half-Lives of *daf-2* and Reference Replicates and Estimation of Mitochondrial Turnover Rates with the Photoswitchable Reporter Dendra2

(A–C, E–H, and J–M) Heatmap representation of individual protein half-lives of *daf-2* and reference replicates. The colors indicate a relative decrease (red) or increase (blue) of protein half-life compared with the median of the reference strain (white, 103 hr). Color limits signify the 5th (41 hr) and the 95th (291 hr) percentile. Each tile represents a biological replicate. p Values were obtained from the moderated t test implemented in the *limma* R package and adjusted for multiple testing according to Benjamini and Hochberg's method. Asterisks indicate significant differences between both strains. *$p < 0.05$, **$p < 0.01$, ***$p < 0.001$, respectively. (D) Confocal images of *jrIs5* transgenic worms expressing Dendra2 under the constitutive *rps-0* promotor and targeted to the mitochondria with the mitochondrial localization signal of *gas-1*. Left: overview of Dendra2-expressing worms. Scale bar, 100 μm. Right: detail of the midsection of the body. Scale bar, 10 μm. (I) Linear regression of the decline in red Dendra2 fluorescence after photoconversion in reference versus *daf-2* strains (F-test, $p < 0.0001$). Source data are available in Table S4.

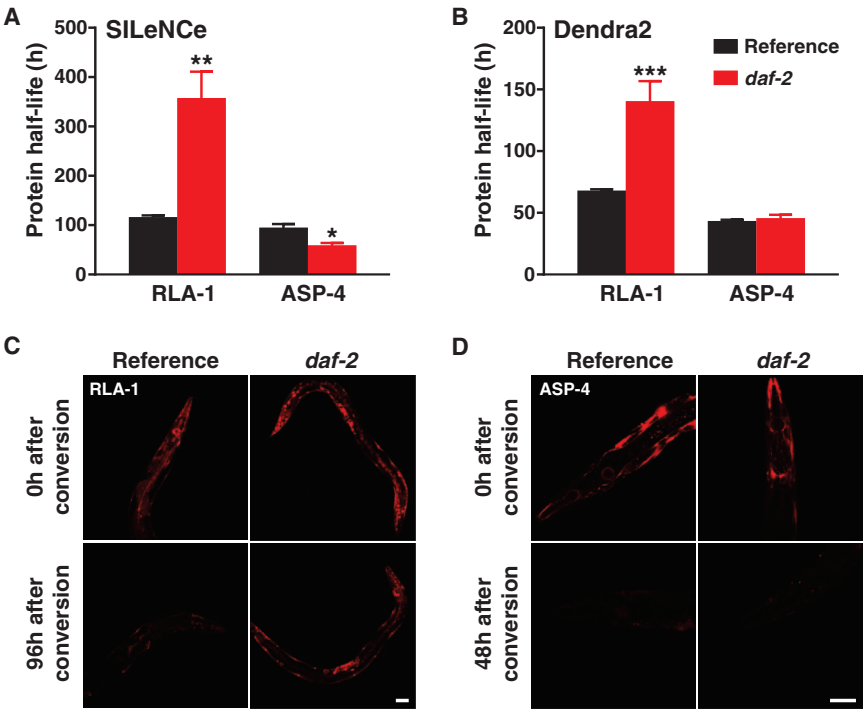

Figure 7. Validation of the SILeNCe Method with the Dendra2 Approach

(A and B) Protein half-lives of RLA-1 and ASP-4, estimated via SILeNCe pulse labeling (A) and the Dendra2 pulse-chase method (B). Red fluorescence decline was determined in *glp-4 daf-2* worms expressing RLA-1::Dendra2 and ASP-4::Dendra2 translation reporters and treated with *daf-16* (reference) and empty vector (L4440) RNAi (*daf-2*) (minimum six individually tracked worms per condition; two-sample Student's t test; $p = 0.0019$ and $p = 0.6278$ for RLA-1 and ASP-4, respectively). Error bars are SEM.

(C and D) Representative confocal images of *glp-4 daf-2;rla-1p::rla-1::Dendra2* (C) and *glp-4 daf-2; asp-4p::asp-4::Dendra2* (D) transgenic worms grown on *daf-16* RNAi (reference) and empty vector L4440 (*daf-2*). Images were taken 96 hr (RLA-1) and 48 hr (ASP-4) after photoconversion. Scale bars, 20 μm.

2007; Pan et al., 2007; Stout et al., 2013; Syntichaki et al., 2007; Van Raamsdonk and Hekimi, 2009; Yang et al., 2007). Therefore, we hypothesized that, in *daf-2* mutants, energy is saved by downregulation of turnover of the majority of proteins and reinvested in prioritized turnover of specific proteins that are crucial to somatic maintenance. To that end, we investigated the turnover dynamics of individual proteins using a SILeNCe metabolic labeling method. Contrary to our hypothesis, we did not discover a delineated set of proteins with turnover priority in *daf-2* mutants. The majority of the detected proteins (56%) exhibit prolonged half-lives in *daf-2*, whereas turnover of the remaining proteins is unchanged. Only three proteins (CPN-3, ASP-4, and VIT-6) display marginally significant higher turnover rates in *daf-2*, but they lack a clear biological relationship. This dramatic change in protein turnover in long-lived *daf-2* was also observed in a parallel study (Visscher et al., 2016 [this issue of *Cell Reports*]).

One of our most notable observations is the drastic slowdown in turnover of the translation machinery in *daf-2* mutants. This slowdown coincides with decreased levels of ribosomal proteins and enzymes with predicted function in ribosome assembly and biogenesis we and others observed earlier (Depuydt et al., 2013; Stout et al., 2013; Walther et al., 2015) and probably relates to the decreased protein synthesis rates in this mutant. In line with this, we also observed a dispersed organization of the RER cisternae with reduced ribosomal count in long-lived *daf-2* worms, which is considered a sign of diminished protein translation (Hansen et al., 2007). Corroborating this is a recent work suggesting a specific translational block in *daf-2* by specific binding of the long non-coding RNA *tts-1* to the ribosomes (Essers et al., 2015). Our observation of decreased protein turnover in *daf-2* mutants is not entirely surprising. The insulin/IGF1 signaling pathway is a main activator of anabolic metabolism; hence, it is conceivable that mutants in this pathway show reduced protein turnover. This reduction allows the worm to save much energy, which may be diverted to other processes that support longevity, such as the synthesis of trehalose, a chemical chaperone that stabilizes membranes and proteins, for which a role in *daf-2* longevity has already been shown (Depuydt et al., 2016; Honda et al., 2010). Moreover, this mutant displays reduced protein degradation activity (Stout et al., 2013), although recent work challenges this finding (Walther et al., 2015). The overall slow protein turnover agrees with the hyperfunction theory, stating that aging is caused by excess biosynthesis (hypertrophy) (Blagosklonny, 2012; Gems and de la Guardia, 2013). Thus, inhibited insulin/IGF-1 signaling reduces anabolic pathways, which, in turn, lowers hypertrophy, decelerating the onset of its related pathologies.

Earlier, it has been shown that reduced insulin/IGF-1 signaling and dietary restriction rely on autophagy to extend the lifespan (Hansen et al., 2008; Meléndez et al., 2003). Hence, the preserved turnover rates of lysosomal proteins might be crucial to sustain autophagy in *daf-2* mutants. However, our data do not support increased bulk protein degradation because most protein half-lives are prolonged or unchanged in *daf-2*. The turnover rates of lysosomal hydrolases are among the fastest found in the cell, which can be explained by the fact that the lysosomal lumen is a strong proteolytic environment in which accidental breakdown of lysosomal components is to be expected. Opposite to these hydrolases, subunits of the V-type ATPase proton pumps, present in the lysosomal membrane, undergo slow turnover, indicating that lysosomes, apart from their content, are not rapidly replaced as a whole. Also, V-type ATPase subunits are part of large complexes that may be intrinsically more stable and resilient to protein breakdown. One remarkable exception is the subunit C homolog VHA-11, which is known to reversibly dissociate from this complex in yeast cells (Iwata et al., 2004).

It shows extremely fast turnover in the reference strain, which is even enhanced in *daf-2* mutants. V1/V0 dissociation is thought to be an energy-conserving response (Kane, 2006), and recent work shows a general role of V-type ATPase complexes in controlling metabolic programs (Zhang et al., 2014). It is possible that VHA-11 functions as an energy-dependent switch, downregulating lysosomal acidification and protein degradation in the *daf-2* mutant. More detailed evaluation of a lysosomal role in the regulation of protein metabolism in *daf-2* is necessary.

Similar to lysosomes, we detected a clear discrepancy in turnover between free and membrane-bound mitochondrial proteins. In addition, the half-lives of mitochondrial proteins vary widely, and no uniformity is found within biochemical pathways. This variability in turnover suggests that mitophagy is not the predominant process for elimination of mitochondrial proteins in *C. elegans* under normal conditions. Matrix proteases and extra-mitochondrial degradation mechanisms are likely co-responsible for mitochondrial protein dynamics (Lau et al., 2012).

Our data disprove that *daf-2* longevity is supported by enhanced mitochondrial turnover rates because the majority of protein half-lives in this organelle are downregulated. One may argue that this is because *daf-2* worms activate their antioxidant defense systems (Honda and Honda, 1999), making the worms less dependent on high turnover of mitochondrial components to avoid damage accumulation. Although we found lower levels of methionine oxidation in the *daf-2* LC-MS/MS data, it should be noted that levels of oxidative damage in mitochondria of young adult wild-type and *daf-2* animals are similar (Brys et al., 2010) and that in vivo hydrogen peroxide production in the muscle is not altered in young adult *daf-2* (Knoefler et al., 2012). Moreover, expression of *sod* is not required for lifespan extension in *daf-2* mutants (Doonan et al., 2008). Despite their low turnover, *daf-2* mitochondria are highly abundant (Depuydt et al., 2013) and show enhanced coupling (Brys et al., 2010). Our previous experiments suggest that, in this mutant, oxidative phosphorylation may be supported by anaerobic mitochondrial pathways (Brys et al., 2010). Although our data challenge extensive recycling of mitochondrial components in the long-lived *daf-2*, selective and specific autophagy of damaged mitochondria might be necessary for its increased lifespan, as suggested recently (Palikaras et al., 2015).

Proteins of the muscle contractile apparatus undergo extremely slow turnover in both reference and *daf-2* worms. Despite their high abundance, half-lives of myosin class II heavy-chain proteins could not be estimated, which is indicative of rare replacement events. These results are consistent with those reported in recent work on protein synthesis during the *C. elegans* lifespan (Vukoti et al., 2015), reporting the slow appearance of newly synthesized motility-related proteins. Although reduced insulin/IGF1 signaling is often associated with muscle atrophy in mammalian systems (Sandri et al., 2004), our previous work showed a highly preserved biomass of striated body wall muscle in *daf-2* compared with the reference strain (Depuydt et al., 2013). In addition, the upkeep of mitochondrial proteins further supports the maintenance of muscle functionality in these mutants. These findings do not exclude the possibility that non-filamental muscle proteins undergo more rapid and even enhanced turnover in *daf-2*, as suggested in a study using a LacZ reporter (Szewczyk et al., 2007). Cytoskeletal components that are not restricted to muscle cells show medium turnover rates, for which only alpha-tubulins are significantly attenuated in *daf-2*, suggesting slightly reduced cellular dynamics in these mutants compared with the reference strain.

Fast to moderate turnover was detected for proteins involved in cytoprotective mechanisms in reference worms. Although microarray studies show strong DAF-16-mediated upregulation of stress-related genes (McElwee et al., 2003; Murphy et al., 2003), several HSPs are downregulated at the protein level (Depuydt et al., 2013) and show a prolonged half-life in *daf-2* mutants in this study. The slow turnover of these chaperones could be related to the recent observation that small HSPs are mostly enriched in the insoluble fraction of old *daf-2* worms, playing a role in protective aggregate formation to maintain proteome balance (Walther et al., 2015). However, it is currently not clear whether these phenomena would be of any significance in the young worms used in our study. Nevertheless, some cytoprotective proteins do show unchanged fast turnover, implicating the complex and specific regulation of stress proteins in *daf-2* mutants.

In summary, we observed an overall slowdown of protein turnover in long-lived *daf-2* worms using a SILeNCe approach. Most prominently, this was reflected in, and probably caused by, drastic lowering of translation machinery turnover in *daf-2*. In agreement with our observations, researchers demonstrated extended ribosomal and mitochondrial half-lives in long-lived, calorie-restricted mice (Karunadharma et al., 2015; Price et al., 2012). Hence, it seems that high protein turnover is not essential to support lifespan extension, but it is still unclear whether the observed slowdown of protein turnover is a causal factor. Recent evidence showing that alleviation of protein synthesis inhibition in *daf-2* mutants partially rescues its longevity phenotype strongly supports this causal relation (Essers et al., 2015). Reduced protein turnover may be related to some typical features of the *daf-2(e1370)* mutant, including reduced food uptake, altered amino acid metabolism, and a lower energetic flux. The *Eat* phenotype, and thus diminished amino acid uptake and likely lower tRNA loading, particularly typify *daf-2* physiology, which possibly supports silenced anabolism and, consequently, decreased global proteome turnover (Davies et al., 2015; Depuydt et al., 2014; Fuchs et al., 2010). Although these aspects of *daf-2* physiology could confound pulse-chase analysis of protein turnover, we validated that limited label uptake or amino acid reutilization was not causal to the reduced turnover measured in our ^{35}S and SILeNCe experiments. This was done by the Dendra2 approach, which is not influenced by label uptake and reutilization. Of note, the absolute protein half-lives resulting from the Dendra2 method differ from those estimated by the SILeNCe approach. This discrepancy originates from differences in parameters used for the calculation of the protein half-lives. In the SILeNCe experiment, half-life is based on synthesis and degradation dynamics (^{15}N incorporation versus ^{14}N loss), whereas the Dendra2 method relies on degradation rates. Nevertheless, relative patterns of protein half-lives are consistent in both approaches. Low protein turnover does not lead to an inferior proteome in *daf-2* worms, as shown by their well-maintained muscle mass (Depuydt et al., 2013) and mitochondrial function (Brys et al., 2010), locomotive ability

(Gems et al., 1998), and metabolic capacity upon mechanical stimulation (Braeckman et al., 2002). Therefore, we believe that reduced insulin/IGF-1 signaling results in an energy-saving state along with the improved protection of proteins. The preserved somatic integrity in *daf-2* possibly relies on chemical chaperones (Depuydt et al., 2016; Honda et al., 2010) or small heat shock proteins (Walther et al., 2015). Our findings and suggestions are also compatible with the hyperfunction theory, which proposes that the attenuation of protein synthesis might reduce hypertrophy, thereby retarding the accumulation of irrelevant macromolecules that otherwise cause age-related cellular malfunction (Blagosklonny, 2012; Gems and de la Guardia, 2013).

EXPERIMENTAL PROCEDURES

Strains

GA154 *glp-4(bn2ts)I;daf-2(e1370)III* (long-lived) and GA153 *glp-4(bn2ts)I daf-16(mgDf50)I; daf-2(e1370)III* (reference strain) were kindly provided by David Gems at the University College of London. The strains were maintained as described previously (Depuydt et al., 2013). The transgenic lines generated by biolistic transformation and crossing were *daf-2(e1370)III;jrIs5[unc-119(+) rps-0p::mls::Dendra2]* and *daf-16(m26)I;daf-2(e1370)III; jrIs5[unc-119(+) rps-0p::mls::Dendra2]*. The strains *glp-4(bn2)I;daf-2(e1370)III;jrEx17[rla-1p::rla-1::Dendra2]* and *glp-4(bn2)I;daf-2(e1370)III;jrEx18[asp-4p::asp-4::Dendra2]* were created by microinjection.

SILeNCe

Metabolic ^{15}N and ^{14}N Labeling of the Escherichia coli *Bacteria*

E. coli K12 was freshly grown overnight at 37°C while shaking at 120 rpm in minimal medium containing 42 mM Na_2HPO_4, 22 mM $KHPO_4$, 9 mM NaCl, trace elements (17 mM EDTA, 3.1 mM $FeCl_3 \cdot 6H_2O$, 0.62 mM $ZnCl_2$, 0.076 mM $CuCl_2 \cdot 2H_2O$, 0.042 mM $CoCl_2 \cdot 6H_2O$, 0.16 mM H_3BO_3, and 0.0068 mM $MnCl_2 \cdot 6H_2O$), glucose 20% (w/v), 1 mM $MgSO_4$, 0.3 mM $CaCl_2$, 0.0041 mM biotin, 0.0033 mM thiamin, and 93 mM ^{15}N- or ^{14}N-containing NH_4Cl (0.22-μm filter, sterilized). Fully labeled bacterial cultures were obtained by inoculating a single colony with an inoculation loop into 250 ml of minimal medium. Overnight cultures reached an optical density of approximately 1.5 (A_{550}) and were concentrated 50-fold.

Culturing and Sampling of C. elegans

Synchronized L1 nematodes were plated on nitrogen-free agarose (1.2%) plates containing NaCl (0.3%), cholesterol (0.0005%), 1 mM $CaCl_2$, 1 mM $MgSO_4$, and 25 mM K_2HPO_4/KH_2PO_4 (pH 6.0) and a lawn of freshly grown ^{14}N-labeled *E. coli* K12 cells. To prevent dauer formation, *glp-4(bn2ts)I; daf-2(e1370)III* were grown at 17°C until the third larval stage (L3) and then switched to 24°C for the remainder of the experiment. Worms that had freshly molted to adults (adult day 0) were washed three times and transferred into culture flasks (not exceeding 1,500 worms/ml) containing S-basal (100 mM NaCl, 50 mM potassium phosphate [pH 6.0]), 12.93 μM cholesterol, 75 μM 5-fluoro-2′-deoxyuridine (Acros Organics), and ^{14}N-labeled *E. coli* K12 cells (A_{550} = 1.0). On day 2 of adulthood, worms were collected and washed thoroughly (2× S-basal, 1× S-basal containing 2.5 mM EDTA, 2× S-basal) to remove bacteria. Next, worms were pulsed in new culture flasks containing S-basal, 12.93 μM cholesterol, 75 μM 5-fluoro-2′-deoxyuridine (Acros Organics), and ^{15}N-labeled *E. coli* K12 cells (A_{550} = 1.0). From this moment, worms were sampled after 0, 15, 20, 27, 40, and 72 hr of ^{15}N pulsing. Animals were washed thoroughly (2× S-basal, 1× S-basal containing 2.5 mM EDTA, 2× S-basal) to remove bacteria, after which dead worms were removed via Percoll (Sigma-Aldrich) washing. The worm pellet was resuspended in 200 μl denaturing solution (8 M urea, 1 mM EDTA, 10 mM DTT, and 50 mM TrisHCl [pH 8.0]) and immediately dripped into liquid nitrogen and stored at −80°C. The sample size was chosen based on our previous study (Depuydt et al., 2013). We sampled all the different post-pulse time points in five biological replicates for both *glp-4(bn2ts)I daf-16(mgDf50)I; daf-2(e1370)III* and *glp-4(bn2ts)I; daf-2(e1370)III*.

Quantitative Proteomics

Randomized Study Design

Samples were processed in batches comprising all the biological replicates of both reference and *daf-2* worms sampled at one time point post-labeling. Samples within a batch were analyzed blindly and in random order (Table S3).

Preparation of the Tryptic Peptide Samples

The frozen worm beads (~1,500 worms in denaturing solution) were homogenized using a BioPulverizer (BioSpec) pre-conditioned in liquid nitrogen. The fine powder was recovered into a 1.5-ml tube, thawed, centrifuged (2 min, 5,000 rpm), and sonicated for 30 s in a 5510 Branson ultrasonic water bath (Branson Ultrasonics). Protein concentrations were determined using a Coomassie assay. Further sample processing steps, LC/MS peptide identification, and data processing strategies are provided in the Supplemental Experimental Procedures.

Functional Analysis and Data Visualization

The UniProtKB Protein Knowledgebase (UniProt 2015), the Database for Annotation, Visualization, and Integrated Discovery (DAVID 2014) (Dennis et al., 2003), and Wormbase (version WS246) were used for protein annotation and evaluation of functionally and spatially related proteins (Table S4). Heatmap visualization of different protein half-lives was done with the MultiExperiment Viewer, part of the TM4 microarray software suite (Saeed et al., 2003). Euclidean distances between proteins were calculated and used as a distance metric in a hierarchical clustering analysis (HCA) together with an average pairwise distance as linkage method. Graphs and statistical tests (including tests for normality) were performed with GraphPad Prism version 6.05 for Windows (GraphPad).

Correlation Analysis of Protein Abundance and Half-Lives

In total, 167 common proteins were detected comparing the SILeNCe dataset with the previously obtained proteomic dataset of Depuydt et al. (2013) (Table S2). The "dietary restriction" condition was removed from the latter, and the set was re-normalized. Pearson correlation analysis was performed between $\log_2$-transformed ratios of protein abundance and protein half-lives ($\log_2$ fold change) (GraphPad Prism version 6.05 for Windows).

Dendra2

jrIs5[unc-119(+)rps-0p::mls::Dendra2] was created using biolistic transformation (PDS-1000/He System, Bio-Rad) to study mitochondrial turnover. This reporter is a concatenate of the ubiquitous ribosomal protein subunit promoter *rps-0p*, the *gas-1* mitochondrial localization sequence, and the Dendra2 gene (Evrogen). This transgenic strain was crossed with the *daf-2(e1370)III* mutant. The reference strain was obtained by crossing the latter strain with the *daf-16(m26)I* genetic background. An device emitting intense violet light was hand-built (4 × 20 W, 415- to 420-nm light emitting diodes (LEDs), Zhuhai Tianhui Electronics) for mass photoconversion of worms without affecting lifespan and fecundity (data not shown). Residual UV and heat produced by the LEDs were eliminated using UV filters and heat mirrors, respectively. Day 1 adult worms were photoconverted during 30 min and, subsequently, red Dendra2 fluorescence intensity was measured at regular time points using a Victor^2 1420 multilabel counter (PerkinElmer). Fluorescence was normalized to protein content as determined using a BCA protein assay kit (Thermo Scientific). The slopes, representing mitochondrial Dendra2 turnover, were evaluated in GraphPad Prism using linear regression analysis.

Ribosomal and lysosomal protein degradation was assayed by microinjecting an *rla-1p::rla-1::Dendra2* or *asp-4p::asp-4::Dendra2* construct containing a 2-kb upstream and 1-kb downstream sequence of the respective gene in the *glp-4(bn2)I;daf-2(e1370)III* mutant. Synchronized L1 worms were grown on nematode growth medium (NGM) plates seeded with freshly induced RNAi bacteria (L4440 empty vector and *daf-16*), incubated at 17°C until the third larval stage (L3), and then switched to 24°C for the remainder of the experiment. *daf-16* RNAi resulted in the expected abrogation of the longevity phenotype of *glp-4;daf-2* worms (Figure S5). On the second day of adulthood, worms (n = 6/condition) were photoconverted and immediately imaged using confocal microscopy. Subsequently, worms were rescued and replaced on fresh RNAi plates. After 48 or 96 hr, the same individuals were re-imaged using the same camera settings specific for each animal. Confocal images were acquired using a Nikon TiE-C2 confocal microscope with objectives Plan 4× 0.10 chrome-free infinity-corrected (CFI) (numerical aperture [NA] 0.1, dry),

20× CFI Plan Apochromat VC (NA 0.75, dry), and Plan Apo VC 60×A WI differential interference contrast (DIC) N2 (NA 1.20, water immersion [WI]) and the NIS Elements imaging software (version 4.13.03). The Dendra2 fluorochrome was excited with a 561-nm solid-state laser, and the emission was collected with a 605/55-nm band-pass filter. The mean intensity per pixel of red Dendra2 fluorescence was determined with ImageJ (Schneider et al., 2012). Protein half-lives were calculated as the fractional decline of red fluorescence per hour based on two measured time points.

Data Availability

The mass spectrometry proteomics data have been deposited to the ProteomeXchange Consortium (Vizcaíno et al., 2014) via the PRIDE partner repository with the dataset identifiers PXD002317 and 10.6019/PXD002317.

ACCESSION NUMBERS

The accession numbers for the mass spectrometry proteomics data reported in this paper are ProteomeXchange Consortium: PXD002317 and 10.6019/PXD002317.

SUPPLEMENTAL INFORMATION

Supplemental Information includes Supplemental Experimental Procedures, five figures, and four tables and can be found with this article online at http://dx.doi.org/10.1016/j.celrep.2016.07.088.

AUTHOR CONTRIBUTIONS

I.D., V.P., and B.P.B. designed the experiments. I.D., L.V., and H.C. carried out the experiments. I.D. performed the sample preparation, and V.P. carried out the instrumental analysis. I.D., V.P., and B.P.B. analyzed and interpreted the data. G.D., I.D., and A.V. designed and generated the Dendra2 transgenic lines. I.D. and B.P.B. wrote the manuscript, and this was further edited by G.D., V.P., R.D.S., and B.P.B.

ACKNOWLEDGMENTS

We thank the Gems laboratory for providing the strains GA153 and GA154. We are grateful to Caroline Vlaeminck and Renata Coopman for technical support with the SILeNCe experiments. We also acknowledge Myriam Claes for assisting with TEM imaging and Marjolein Couvreur for her assistance with the microinjections. I.D. acknowledges a Ph.D. grant from the Fund for Scientific Research – Flanders, Belgium (FWO11/ASP/031). H.C. acknowledges CSC Ph.D. Grant 201207650008 with BOF co-funding from Ghent University (01SC0313). Portions of this work were supported by NIH P41GM103493 (to R.D.S.). The experimental work described here was performed in the Environmental Molecular Sciences Laboratory, a national scientific user facility sponsored by the DOE and located at Pacific Northwest National Laboratory, which is operated by Battelle Memorial Institute for the DOE under Contract DE-AC05-76RL0 1830.

Received: August 17, 2015
Revised: April 8, 2016
Accepted: July 1, 2016
Published: September 13, 2016

REFERENCES

Arantes-Oliveira, N., Apfeld, J., Dillin, A., and Kenyon, C. (2002). Regulation of life-span by germ-line stem cells in Caenorhabditis elegans. Science *295*, 502–505.

Ayyadevara, S., Dandapat, A., Singh, S.P., Siegel, E.R., Shmookler Reis, R.J., Zimniak, L., and Zimniak, P. (2007). Life span and stress resistance of Caenorhabditis elegans are differentially affected by glutathione transferases metabolizing 4-hydroxynon-2-enal. Mech. Ageing Dev. *128*, 196–205.

Blagosklonny, M.V. (2012). Answering the ultimate question "what is the proximal cause of aging?". Aging (Albany, N.Y.) *4*, 861–877.

Braeckman, B.P., Houthoofd, K., and Vanfleteren, J.R. (2002). Assessing metabolic activity in aging Caenorhabditis elegans: concepts and controversies. Aging Cell *1*, 82–88, discussion 102–103.

Brys, K., Castelein, N., Matthijssens, F., Vanfleteren, J.R., and Braeckman, B.P. (2010). Disruption of insulin signalling preserves bioenergetic competence of mitochondria in ageing Caenorhabditis elegans. BMC Biol. *8*, 91.

Claydon, A.J., and Beynon, R. (2012). Proteome dynamics: revisiting turnover with a global perspective. Mol. Cell. Proteomics *11*, 1551–1565.

Davies, S.K., Bundy, J.G., and Leroi, A.M. (2015). Metabolic Youth in Middle Age: Predicting Aging in Caenorhabditis elegans Using Metabolomics. J. Proteome Res. *14*, 4603–4609.

Dennis, G., Jr., Sherman, B.T., Hosack, D.A., Yang, J., Gao, W., Lane, H.C., and Lempicki, R.A. (2003). DAVID: Database for Annotation, Visualization, and Integrated Discovery. Genome Biol. *4*, 3.

Depuydt, G., Xie, F., Petyuk, V.A., Shanmugam, N., Smolders, A., Dhondt, I., Brewer, H.M., Camp, D.G., Smith, R.D., and Braeckman, B.P. (2013). Reduced insulin/IGF-1 signaling and dietary restriction inhibit translation but preserve muscle mass in Caenorhabditis elegans. Mol. Cell. Proteomics *12*, 3624–3639.

Depuydt, G., Xie, F., Petyuk, V.A., Smolders, A., Brewer, H.M., Camp, D.G., 2nd, Smith, R.D., and Braeckman, B.P. (2014). LC-MS proteomics analysis of the insulin/IGF-1-deficient Caenorhabditis elegans daf-2(e1370) mutant reveals extensive restructuring of intermediary metabolism. J. Proteome Res. *13*, 1938–1956.

Depuydt, G., Shanmugam, N., Rasulova, M., Dhondt, I., and Braeckman, B.P. (2016). Increased protein stability and decreased protein turnover in the Caenorhabditis elegans Ins/IGF-1 daf-2 mutant. J Gerontol A Biol Sci Med Sci, Published online February 10, 2016. http://dx.doi.org/10.1093/gerona/glv221.

Doonan, R., McElwee, J.J., Matthijssens, F., Walker, G.A., Houthoofd, K., Back, P., Matscheski, A., Vanfleteren, J.R., and Gems, D. (2008). Against the oxidative damage theory of aging: superoxide dismutases protect against oxidative stress but have little or no effect on life span in Caenorhabditis elegans. Genes Dev. *22*, 3236–3241.

Essers, P.B., Nonnekens, J., Goos, Y.J., Betist, M.C., Viester, M.D., Mossink, B., Lansu, N., Korswagen, H.C., Jelier, R., Brenkman, A.B., and MacInnes, A.W. (2015). A Long Noncoding RNA on the Ribosome Is Required for Lifespan Extension. Cell Rep. Published online January 13, 2015. http://dx.doi.org/10.1016/j.celrep.2014.12.029.

Fuchs, S., Bundy, J.G., Davies, S.K., Viney, J.M., Swire, J.S., and Leroi, A.M. (2010). A metabolic signature of long life in Caenorhabditis elegans. BMC Biol. *8*, 14.

Geillinger, K.E., Kuhlmann, K., Eisenacher, M., Meyer, H.E., Daniel, H., and Spanier, B. (2012). Dynamic changes of the Caenorhabditis elegans proteome during ontogenesis assessed by quantitative analysis with 15N metabolic labeling. J. Proteome Res. *11*, 4594–4604.

Gems, D., and de la Guardia, Y. (2013). Alternative Perspectives on Aging in Caenorhabditis elegans: Reactive Oxygen Species or Hyperfunction? Antioxid. Redox Signal. *19*, 321–329.

Gems, D., Sutton, A.J., Sundermeyer, M.L., Albert, P.S., King, K.V., Edgley, M.L., Larsen, P.L., and Riddle, D.L. (1998). Two pleiotropic classes of daf-2 mutation affect larval arrest, adult behavior, reproduction and longevity in Caenorhabditis elegans. Genetics *150*, 129–155.

Gomez-Amaro, R.L., Valentine, E.R., Carretero, M., LeBoeuf, S.E., Rangaraju, S., Broaddus, C.D., Solis, G.M., Williamson, J.R., and Petrascheck, M. (2015). Measuring Food Intake and Nutrient Absorption in Caenorhabditis elegans. Genetics *200*, 443–454.

Grune, T. (2000). Oxidative stress, aging and the proteasomal system. Biogerontology *1*, 31–40.

Gurskaya, N.G., Verkhusha, V.V., Shcheglov, A.S., Staroverov, D.B., Chepurnykh, T.V., Fradkov, A.F., Lukyanov, S., and Lukyanov, K.A. (2006).

Engineering of a monomeric green-to-red photoactivatable fluorescent protein induced by blue light. Nat Biotechnol *24*, 461–465.

Hansen, M., Taubert, S., Crawford, D., Libina, N., Lee, S.J., and Kenyon, C. (2007). Lifespan extension by conditions that inhibit translation in Caenorhabditis elegans. Aging Cell *6*, 95–110.

Hansen, M., Chandra, A., Mitic, L.L., Onken, B., Driscoll, M., and Kenyon, C. (2008). A role for autophagy in the extension of lifespan by dietary restriction in C. elegans. PLoS Genet. *4*, e24.

Heald, R., and Cohen-Fix, O. (2014). Morphology and function of membrane-bound organelles. Curr. Opin. Cell Biol. *26*, 79–86.

Honda, Y., and Honda, S. (1999). The daf-2 gene network for longevity regulates oxidative stress resistance and Mn-superoxide dismutase gene expression in Caenorhabditis elegans. FASEB J. *13*, 1385–1393.

Honda, Y., Tanaka, M., and Honda, S. (2010). Trehalose extends longevity in the nematode Caenorhabditis elegans. Aging Cell *9*, 558–569.

Houthoofd, K., Braeckman, B.P., Lenaerts, I., Brys, K., Matthijssens, F., De Vreese, A., Van Eygen, S., and Vanfleteren, J.R. (2005). DAF-2 pathway mutations and food restriction in aging Caenorhabditis elegans differentially affect metabolism. Neurobiol. Aging *26*, 689–696.

Hsin, H., and Kenyon, C. (1999). Signals from the reproductive system regulate the lifespan of C. elegans. Nature *399*, 362–366.

Iwata, M., Imamura, H., Stambouli, E., Ikeda, C., Tamakoshi, M., Nagata, K., Makyio, H., Hankamer, B., Barber, J., Yoshida, M., et al. (2004). Crystal structure of a central stalk subunit C and reversible association/dissociation of vacuole-type ATPase. Proc. Natl. Acad. Sci. USA *101*, 59–64.

Kaeberlein, M., Powers, R.W., 3rd, Steffen, K.K., Westman, E.A., Hu, D., Dang, N., Kerr, E.O., Kirkland, K.T., Fields, S., and Kennedy, B.K. (2005). Regulation of yeast replicative life span by TOR and Sch9 in response to nutrients. Science *310*, 1193–1196.

Kane, P.M. (2006). The where, when, and how of organelle acidification by the yeast vacuolar H+-ATPase. Microbiol. Mol. Biol. Rev. *70*, 177–191.

Karunadharma, P.P., Basisty, N., Dai, D.F., Chiao, Y.A., Quarles, E.K., Hsieh, E.J., Crispin, D., Bielas, J.H., Ericson, N.G., Beyer, R.P., et al. (2015). Subacute calorie restriction and rapamycin discordantly alter mouse liver proteome homeostasis and reverse aging effects. Aging Cell *14*, 547–557.

Kenyon, C., Chang, J., Gensch, E., Rudner, A., and Tabtiang, R. (1993). A C. elegans mutant that lives twice as long as wild type. Nature *366*, 461–464.

Knoefler, D., Thamsen, M., Koniczek, M., Niemuth, N.J., Diederich, A.K., and Jakob, U. (2012). Quantitative in vivo redox sensors uncover oxidative stress as an early event in life. Mol. Cell *47*, 767–776.

Krijgsveld, J., Ketting, R.F., Mahmoudi, T., Johansen, J., Artal-Sanz, M., Verrijzer, C.P., Plasterk, R.H., and Heck, A.J. (2003). Metabolic labeling of C. elegans and D. melanogaster for quantitative proteomics. Nat. Biotechnol. *21*, 927–931.

Lau, E., Wang, D., Zhang, J., Yu, H., Lam, M.P., Liang, X., Zong, N., Kim, T.Y., and Ping, P. (2012). Substrate- and isoform-specific proteome stability in normal and stressed cardiac mitochondria. Circ. Res. *110*, 1174–1178.

Lewis, S.E., Goldspink, D.F., Phillips, J.G., Merry, B.J., and Holehan, A.M. (1985). The effects of aging and chronic dietary restriction on whole body growth and protein turnover in the rat. Exp. Gerontol. *20*, 253–263.

Lin, K., Hsin, H., Libina, N., and Kenyon, C. (2001). Regulation of the Caenorhabditis elegans longevity protein DAF-16 by insulin/IGF-1 and germline signaling. Nat. Genet. *28*, 139–145.

McColl, G., Vantipalli, M.C., and Lithgow, G.J. (2005). The C. elegans ortholog of mammalian Ku70, interacts with insulin-like signaling to modulate stress resistance and life span. FASEB J. *19*, 1716–1718.

McElwee, J., Bubb, K., and Thomas, J.H. (2003). Transcriptional outputs of the Caenorhabditis elegans forkhead protein DAF-16. Aging Cell *2*, 111–121.

McElwee, J.J., Schuster, E., Blanc, E., Thomas, J.H., and Gems, D. (2004). Shared transcriptional signature in Caenorhabditis elegans Dauer larvae and long-lived daf-2 mutants implicates detoxification system in longevity assurance. J. Biol. Chem. *279*, 44533–44543.

McElwee, J.J., Schuster, E., Blanc, E., Piper, M.D., Thomas, J.H., Patel, D.S., Selman, C., Withers, D.J., Thornton, J.M., Partridge, L., and Gems, D. (2007). Evolutionary conservation of regulated longevity assurance mechanisms. Genome Biol. *8*, R132.

Meléndez, A., Tallóczy, Z., Seaman, M., Eskelinen, E.L., Hall, D.H., and Levine, B. (2003). Autophagy genes are essential for dauer development and life-span extension in C. elegans. Science *301*, 1387–1391.

Mindell, J.A. (2012). Lysosomal acidification mechanisms. Annu. Rev. Physiol. *74*, 69–86.

Murphy, M.P. (2009). How mitochondria produce reactive oxygen species. Biochem. J. *417*, 1–13.

Murphy, C.T., McCarroll, S.A., Bargmann, C.I., Fraser, A., Kamath, R.S., Ahringer, J., Li, H., and Kenyon, C. (2003). Genes that act downstream of DAF-16 to influence the lifespan of Caenorhabditis elegans. Nature *424*, 277–283.

Palikaras, K., Lionaki, E., and Tavernarakis, N. (2015). Coordination of mitophagy and mitochondrial biogenesis during ageing in C. elegans. Nature *521*, 525–528.

Pan, K.Z., Palter, J.E., Rogers, A.N., Olsen, A., Chen, D., Lithgow, G.J., and Kapahi, P. (2007). Inhibition of mRNA translation extends lifespan in Caenorhabditis elegans. Aging Cell *6*, 111–119.

Price, J.C., Khambatta, C.F., Li, K.W., Bruss, M.D., Shankaran, M., Dalidd, M., Floreani, N.A., Roberts, L.S., Turner, S.M., Holmes, W.E., and Hellerstein, M.K. (2012). The effect of long term calorie restriction on in vivo hepatic proteostatis: a novel combination of dynamic and quantitative proteomics. Mol. Cell. Proteomics *11*, 1801–1814.

Ralser, M., Wamelink, M.M., Kowald, A., Gerisch, B., Heeren, G., Struys, E.A., Klipp, E., Jakobs, C., Breitenbach, M., Lehrach, H., and Krobitsch, S. (2007). Dynamic rerouting of the carbohydrate flux is key to counteracting oxidative stress. J. Biol. *6*, 10.

Rastogi, S., Borgo, B., Pazdernik, N., Fox, P., Mardis, E.R., Kohara, Y., Havranek, J., and Schedl, T. (2015). Caenorhabditis elegans glp-4 encodes a valyl aminoacyl tRNA synthetase. G3 *5*, 2719–2728.

Rattan, S.I. (1996). Synthesis, modifications, and turnover of proteins during aging. Exp. Gerontol. *31*, 33–47.

Ritchie, M.E., Phipson, B., Wu, D., Hu, Y., Law, C.W., Shi, W., and Smyth, G.K. (2015). limma powers differential expression analyses for RNA-sequencing and microarray studies. Nucleic Acids Res. *43*, e47.

Ryazanov, A.G., and Nefsky, B.S. (2002). Protein turnover plays a key role in aging. Mech. Ageing Dev. *123*, 207–213.

Saeed, A.I., Sharov, V., White, J., Li, J., Liang, W., Bhagabati, N., Braisted, J., Klapa, M., Currier, T., Thiagarajan, M., et al. (2003). TM4: a free, open-source system for microarray data management and analysis. Biotechniques *34*, 374–378.

Sandri, M., Sandri, C., Gilbert, A., Skurk, C., Calabria, E., Picard, A., Walsh, K., Schiaffino, S., Lecker, S.H., and Goldberg, A.L. (2004). Foxo transcription factors induce the atrophy-related ubiquitin ligase atrogin-1 and cause skeletal muscle atrophy. Cell *117*, 399–412.

Schneider, C.A., Rasband, W.S., and Eliceiri, K.W. (2012). NIH Image to ImageJ: 25 years of image analysis. Nat. Methods *9*, 671–675.

Shore, D.E., Carr, C.E., and Ruvkun, G. (2012). Induction of cytoprotective pathways is central to the extension of lifespan conferred by multiple longevity pathways. PLoS Genet. *8*, e1002792.

Stout, G.J., Stigter, E.C., Essers, P.B., Mulder, K.W., Kolkman, A., Snijders, D.S., van den Broek, N.J., Betist, M.C., Korswagen, H.C., Macinnes, A.W., and Brenkman, A.B. (2013). Insulin/IGF-1-mediated longevity is marked by reduced protein metabolism. Mol. Syst. Biol. *9*, 679.

Syntichaki, P., Troulinaki, K., and Tavernarakis, N. (2007). Protein synthesis is a novel determinant of aging in Caenorhabditis elegans. Ann. N Y Acad. Sci. *1119*, 289–295.

Szewczyk, N.J., Peterson, B.K., Barmada, S.J., Parkinson, L.P., and Jacobson, L.A. (2007). Opposed growth factor signals control protein degradation in muscles of Caenorhabditis elegans. EMBO J. *26*, 935–943.

Taylor, R.C., and Dillin, A. (2011). Aging as an event of proteostasis collapse. Cold Spring Harb. Perspect. Biol. *3*, 3.

TeKippe, M., and Aballay, A. (2010). C. elegans germline-deficient mutants respond to pathogen infection using shared and distinct mechanisms. PLoS ONE *5*, e11777.

Terasaki, M., Shemesh, T., Kasthuri, N., Klemm, R.W., Schalek, R., Hayworth, K.J., Hand, A.R., Yankova, M., Huber, G., Lichtman, J.W., et al. (2013). Stacked endoplasmic reticulum sheets are connected by helicoidal membrane motifs. Cell *154*, 285–296.

Van Raamsdonk, J.M., and Hekimi, S. (2009). Deletion of the mitochondrial superoxide dismutase sod-2 extends lifespan in Caenorhabditis elegans. PLoS Genet. *5*, e1000361.

Vázquez-Martínez, R., Díaz-Ruiz, A., Almabouada, F., Rabanal-Ruiz, Y., Gracia-Navarro, F., and Malagón, M.M. (2012). Revisiting the regulated secretory pathway: from frogs to human. Gen. Comp. Endocrinol. *175*, 1–9.

Visscher, M., De Henau, S., Wildschut, M.H.E., van Es, R.M., Dhondt, I., Kemmeren, P., Nollen, E.A., Braeckman, B.P., Burgering, B.M.T., Vos, H.R., and Dansen, T.B. (2016). Human iNKT cells promote protective inflammation by inducing oscillating purinergic signaling in monocyte-derived DCs. Cell Rep. *16*, this issue, 3041–3051.

Vizcaíno, J.A., Deutsch, E.W., Wang, R., Csordas, A., Reisinger, F., Ríos, D., Dianes, J.A., Sun, Z., Farrah, T., Bandeira, N., et al. (2014). ProteomeXchange provides globally coordinated proteomics data submission and dissemination. Nat. Biotechnol. *32*, 223–226.

Vukoti, K., Yu, X., Sheng, Q., Saha, S., Feng, Z., Hsu, A.L., and Miyagi, M. (2015). Monitoring newly synthesized proteins over the adult life span of Caenorhabditis elegans. J. Proteome Res. *14*, 1483–1494.

Wallimann, T., Tokarska-Schlattner, M., and Schlattner, U. (2011). The creatine kinase system and pleiotropic effects of creatine. Amino Acids *40*, 1271–1296.

Walther, D.M., Kasturi, P., Zheng, M., Pinkert, S., Vecchi, G., Ciryam, P., Morimoto, R.I., Dobson, C.M., Vendruscolo, M., Mann, M., and Hartl, F.U. (2015). Widespread Proteome Remodeling and Aggregation in Aging C. elegans. Cell *161*, 919–932.

Wang, M., Herrmann, C.J., Simonovic, M., Szklarczyk, D., and von Mering, C. (2015). Version 4.0 of PaxDb: Protein abundance data, integrated across model organisms, tissues, and cell-lines. Proteomics *15*, 3163–3168.

Ward, W.F. (2000). The relentless effects of the aging process on protein turnover. Biogerontology *1*, 195–199.

Yang, W., Li, J., and Hekimi, S. (2007). A Measurable increase in oxidative damage due to reduction in superoxide detoxification fails to shorten the life span of long-lived mitochondrial mutants of Caenorhabditis elegans. Genetics *177*, 2063–2074.

Yorimitsu, T., and Klionsky, D.J. (2005). Autophagy: molecular machinery for self-eating. Cell Death Differ. *12* (*Suppl 2*), 1542–1552.

Young, V.R., Steffee, W.P., Pencharz, P.B., Winterer, J.C., and Scrimshaw, N.S. (1975). Total human body protein synthesis in relation to protein requirements at various ages. Nature *253*, 192–194.

Zhang, C.S., Jiang, B., Li, M., Zhu, M., Peng, Y., Zhang, Y.L., Wu, Y.Q., Li, T.Y., Liang, Y., Lu, Z., et al. (2014). The lysosomal v-ATPase-Ragulator complex is a common activator for AMPK and mTORC1, acting as a switch between catabolism and anabolism. Cell Metab. *20*, 526–540.

Cell Reports, Volume *16*

Supplemental Information

FOXO/DAF-16 Activation Slows Down Turnover of the Majority of Proteins in *C. elegans*

Ineke Dhondt, Vladislav A. Petyuk, Huaihan Cai, Lieselot Vandemeulebroucke, Andy Vierstraete, Richard D. Smith, Geert Depuydt, and Bart P. Braeckman

Supplemental Figures

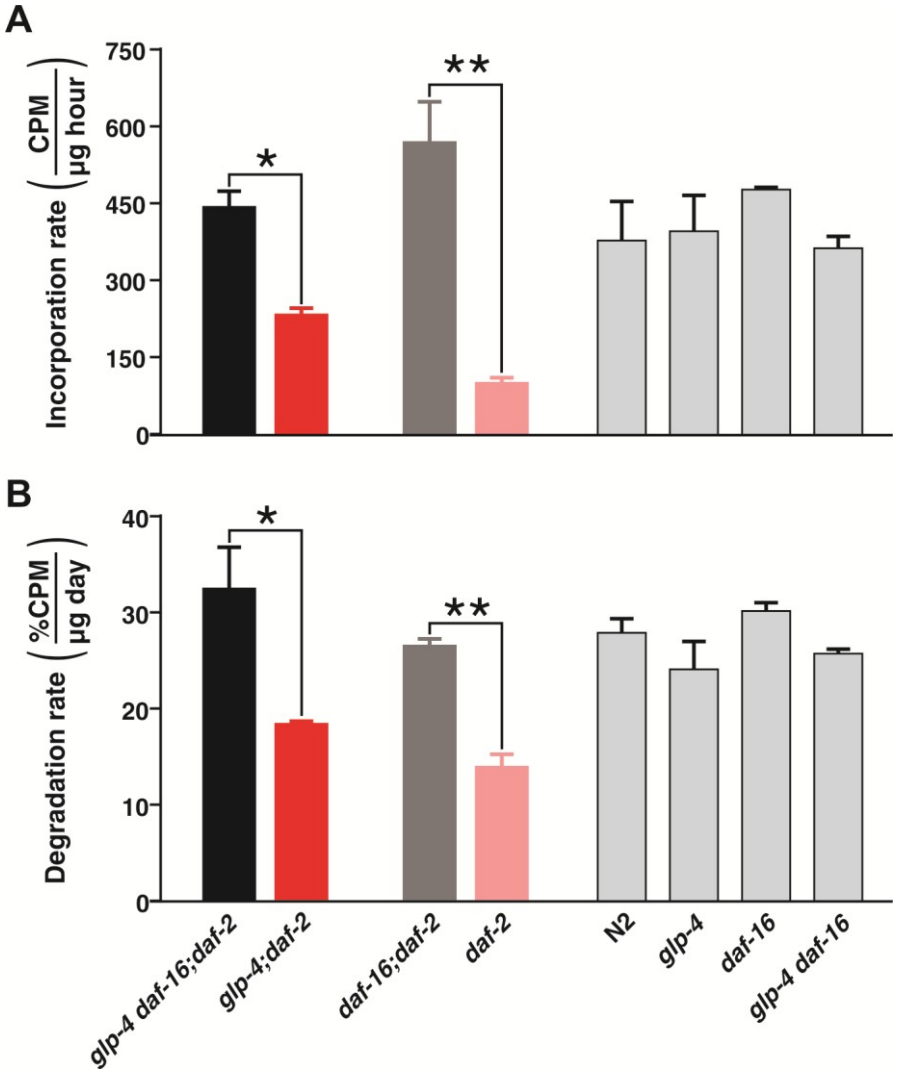

Figure S1. Classical ^{35}S pulse-chase experiment corroborates overall slow-down of protein turnover, Related to the first and second paragraph of the Results.

The ^{35}S incorporation rate in proteins of worms pulsed with ^{35}S-labeled *E. coli* bacteria (A) and the daily fractional decline of ^{35}S in worm proteins during chase (B) for strains used in the SILeNCe experiments and genetic controls. Long-lived worms are indicated in red. $^{(*)}$ $P < 0.05$, $^{(**)}$ $P < 0.01$, for Student's two-sided unpaired *t*-test. Errors are SEM of three independent biological replicates.

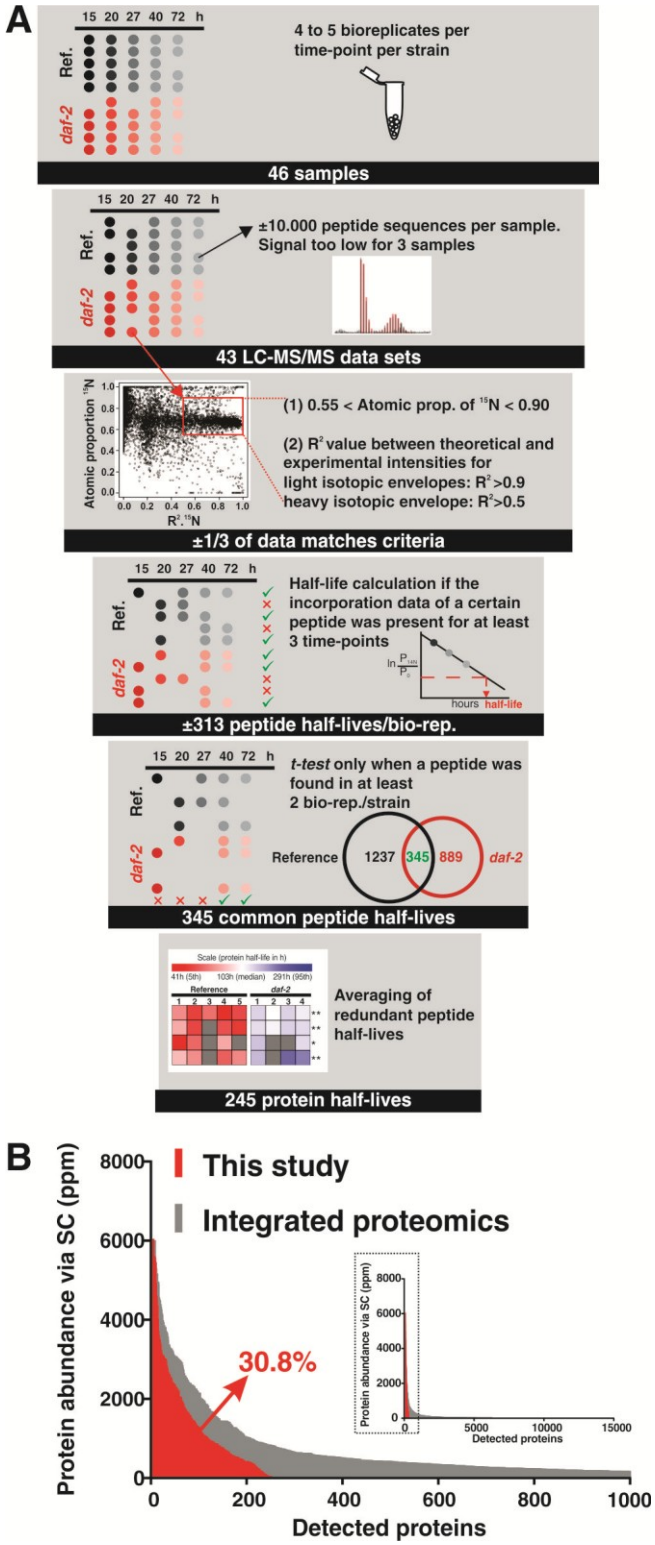

Figure S2. Workflow and data filtering, Related to Figure 1.

(A) Schematic representation of the proteomic analysis illustrating the conservative approach to compare protein half-lives between reference and long-lived *daf-2* worms.

(B) Abundance of proteins detected in ten integrated deep proteomic studies on *C. elegans* (gray) and this study (red). Protein abundance was determined via spectral counting and re-scaled to parts per million (datasets are available online via http://pax-db.org). Proteins in this study add up to 30.8% of total protein abundance of the integrated deep proteomics studies.

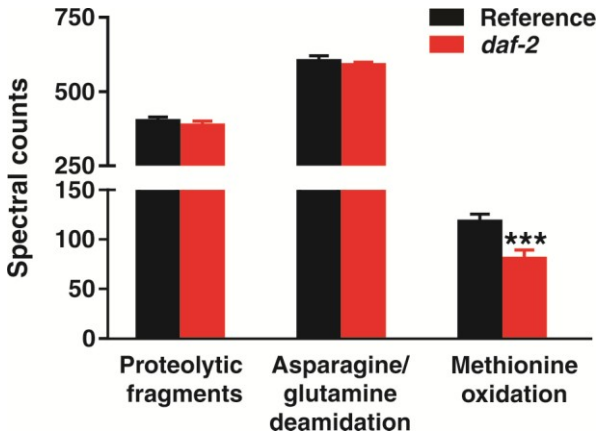

Figure S3. Protein damage in reference and *daf-2* strains, Related to the second paragraph of the Results.

Assessment of proteolytic damage, protein deamidation and oxidative damage via LC-MS/MS screening at day 2 of adulthood (time-point 0 hour post pulse). Barplots reflect the counts of spectra matching to peptides with the presence of proteolytic fragments, asparagine/glutamine deamidation and methionine oxidation. Errors are SEM of five independent biological replicates.

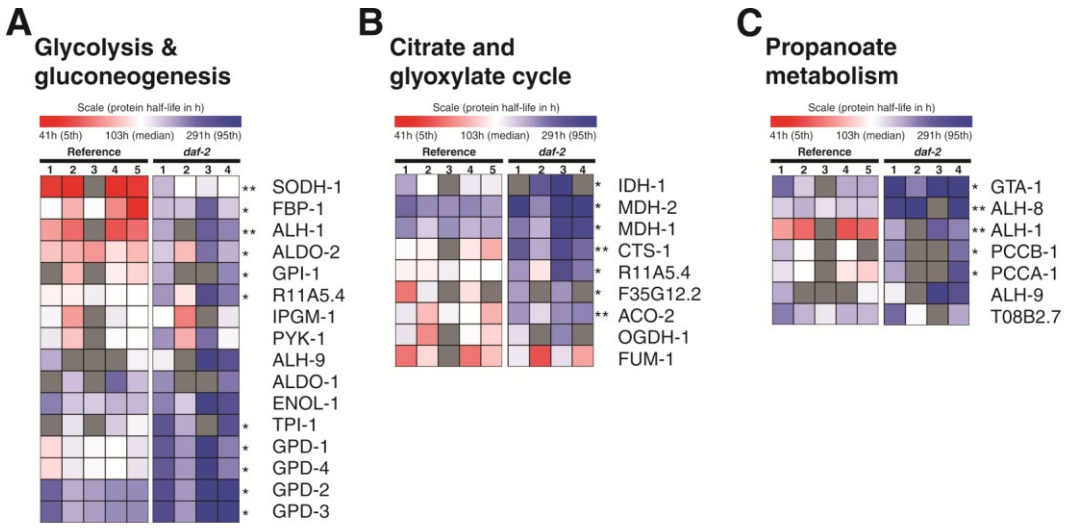

Figure S4. Turnover of proteins involved in carbohydrate metabolism, Related to Figure 5.

The color bar is limited from the 5th percentile (41 h, red) to the 95th percentile (291 h, blue) of protein half-lives determined in our data set. Median half-life (103 h) is represented in white. Each tile signifies a biological replicate. *P*s were obtained from the moderated *t*-test implemented in the *limma* R package and adjusted for multiple testing according to Benjamini and Hochberg's method. Asterisks indicate significant differences between both strains; $^{(*)}$ $P < 0.05$, $^{(**)}$ $P < 0.01$, respectively.

Source data is available in Table S4.

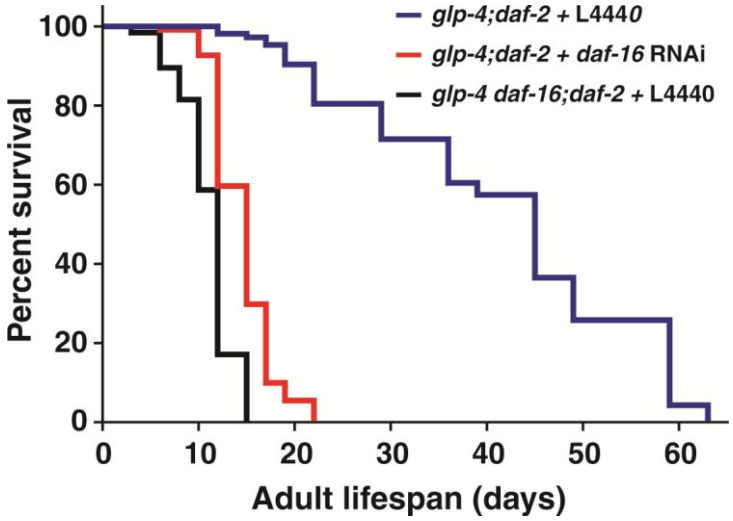

Figure S5. Survival of *glp-4;daf-2* worms subjected to *daf-16* and empty vector (L4440) RNAi, Related to Figure 7.

Supplemental Tables

Table S1. Overview of estimated protein half-lives for the reference and *daf-2* strain, Related to Figure 2.

Table S2. Correlation analysis between protein half-lives and abundance levels, Related to Figure 3.

Table S3. Overview of randomized study design, Related to Figure 1.

Table S4. Summary of protein half-lives of functionally and spatially related proteins for the reference and *daf-2* strain, Related to Figure 4 and 5.

Supplemental Experimental Procedures

^{35}S pulse-chase experiment

E. coli K12 bacteria were grown in low-sulfate medium (44 mM Na_2HPO_4, 22 mM KH_2PO_4, 85 mM NaCl, 20 mM NH_4Cl, 1.25 mg/L thiamine, 0.1% (w/v) glucose, 2 mM $MgCl_2$) (Lewis and Fleming, 1995) supplemented with lysogeny broth medium (1 % final concentration) and 2.5 µCi/mL (^{35}S|sulfate (PerkinElmer, Waltman, MA)). Young worms (day 2 of adulthood) were fed ^{35}S-labeled bacteria and maintained in 10-mL S-basal in tissue culture flasks (approximately 1,000 worms/mL). Sampling procedure, protein isolation and ^{35}S signal quantification (scintillation counting in a Tri-Carb 2800TR Liquid Scintillation Counter from PerkinElmer) were performed as described earlier (Depuydt et al., 2016). Worm protein extracts from five samples taken over an 8-hour pulse period were used to calculate the incorporation rate (protein synthesis) as the upward slope of the ^{35}S signal over time. Protein degradation was measured using a pulse chase experiment, in which worms were pulse labeled by feeding ^{35}S bacteria overnight, washed and chased in S-basal liquid culture containing nonradioactive K12 (OD_{550} = 1.8). The rate of protein degradation was estimated as the fractional decrease of the ^{35}S signal from five samples taken over a 48-hour chase period. The ^{35}S signals (counts per minute or CPM) were normalized to total protein concentration as determined with a BCA Protein Assay Kit (Thermo Scientific, Rockford, IL).

Assessing proteome damage

We assessed the differences in proteome damage from three different perspectives: 1) accumulation of protein fragments resulting from proteolytic cleavage, 2) protein oxidation using oxidation of methionine as a marker, and 3) deamidation of asparagine and glutamine as marker of hydrolysis of functional groups. To that end, we have performed 3 separate MS/MS searches using MS-GF search engine: 1) allowing non-tryptic cleavages, 2) dynamic methionine oxidation and 3) dynamic deamidation on asparagine/glutamine. The optimization of filtering criteria for peptide identification was done using MSnID R/Bioconductor package.

Proteolytic damage

The search results were first separated according to the cleavage patterns of the peptides into fully tryptic, partially tryptic and non-tryptic peptide-to-spectrum matches. The filtering criteria such as MS-GF spectrum E-value (< 5.1e-7) and parent ion mass measurement error (< 7.6 ppm) for the fully tryptic peptide part were optimized to achieve maximum number of peptide identifications (19,006) while constraining unique peptide sequence identification FDR to 1%. This corresponded to 4,475 proteins identified with 6.2% FDR. Further we considered only these as confidently identified proteins for identifying partially and non-tryptic peptides. Thus, the MS/MS identification part containing MS/MS identification was constrained only to proteins identified by tryptic peptides. It was possible to further optimize filtering criteria (MS-GF spectrum E-value < 3.3e-9 and parent ion mass measurement accuracy < 9.3 ppm) to achieve 1% unique peptide sequence FDR for partially tryptic peptides. The 813 partially tryptic peptides matched to 3,921 spectra. We did not identify non-tryptic peptides (both ends non-tryptic) with any reasonable confidence.

Oxidative damage

The search results were first separated into non-modified and peptides containing oxidized methionine. The filtering criteria such as MS-GF spectrum E-value (< 3.2e-8) and parent ion mass measurement error (< 3.1 ppm) for the non-modified peptide part were optimized to achieve maximum number of peptide identifications (19,259) while constraining unique peptide sequence identification FDR to 1%. This was considered the set of confidently identified peptides. Methionine oxidation as majority of other post-translational modification is sub-stoichiometric. Thus any true peptide with oxidized methionine should have matched peptide with the same

sequence. Thus the part of the MS/MS identification containing modification was subset to the confidently identified peptide sequences. As a result we extracted 990 spectra matching to 207 unique peptides with oxidized methionine. The nominal FDR estimate was 0% as not a single resulting peptide sequence matched to a protein with reversed sequence.

Deamidation damage

The search results were first separated into non-modified and peptides containing deamidated arginine or glutamine. The filtering criteria such as MS-GF spectrum E-value (< 2.8e-8) and parent ion mass measurement error (< 3.4 ppm) for the non-modified peptide part were optimized to achieve maximum number of peptide identifications (19,265) while constraining unique peptide sequence identification FDR to 1%. The next step was essentially the same as in the identification of peptides with oxidized methionine. We considered modified peptide only if the non-modified counterpart was confidently identified.

LC-MS/MS sample preparation

We took the aliquots containing 150 µg of protein and readjusted the volume with denaturation buffer. The samples were subjected to cysteine alkylation by 40 mM iodoacetamide for 1 hour at 37°C in dark shaking conditions (900 rpm), 4-fold dilution with 50 mM ammonium bicarbonate (pH 7.8), and digestion with trypsin (3 µg per sample, Promega) for 12 hours at 37°C shaking conditions (400 rpm). Next, tryptic peptide samples were cleaned-up via C-18 SPE columns (Discovery DSC-18, SUPELCO, 52601-U) and concentrations were adjusted to 0.2 µg/µl (Depuydt et al., 2013; Petyuk et al., 2010b).

LC/MS analysis and peptide identification

Each individual sample was analyzed with a constant-pressure capillary HPLC system coupled online to an LTQ Orbitrap mass spectrometer (Thermo Fisher, San Jose, CA) using an electrospray ionization interface. Instrument settings were described previously by Depuydt et al. (2013). The resulting 56 datasets were converted to the mzXML format using MSConvert (settings: --mzXML --32 -z), a part of the ProteoWizard software suite (Kessner et al., 2008). Peptide identification was performed by preprocessing datasets with DeconMSn (Mayampurath et al., 2008), DtaRefinery (Petyuk et al., 2010a) followed by the database search tool MS-GF+ (Kim and Pevzner, 2014). The search was aimed at only light ^{14}N-peptides as we did not anticipate more than 50% label incorporation in such a short labeling pulse. The key MS-GF+ settings are: PMTolerance = 10 ppm; NumMods = 3; StaticMod = C2H3N1O1, C, fix, any, Carbamidomethyl; DynamicMod = None; EnzymeID = 1; IsotopeError = 0.1; NTT = 2; minLenght = 6; maxLenght = 50; minCharge = 1, maxCharge = 4. The results of the MS/MS searches were saved as mzIdentML files. One biological replicate of *daf-2* had to be discarded due to low signal.

Processing 15N/14N LC-MS/MS data

The analysis of the LC-MS/MS datasets was carried out in the R computing environment (version 3.0.2). We built a new package, N14N15 (available from GitHub, https://github.com/vladpetyuk/N14N15), which requires two files as an input: (1) mzXML with raw MS spectra and (2) mzIdentML containing peptide identifications. For the peptides that passed the MS-GF+ confident identification criterion (SpecEvalue < 10^{-9}, < 1% FDR unique peptide level), extracted ion chromatograms were generated for the parent ions in the vicinity of the MS^2 spectrum that yielded identification. After chromatographic peak detection, MS^1 spectra within full width half maximum intensity were summed. Further, given the known elemental composition of the peptide, the summed MS^1 spectrum intensities were fitted with the mixed isotopic distribution assuming one natural and one non-natural proportion of the ^{15}N isotope. The peptides that fitted to the ^{14}N/^{15}N isotopic distribution were filtered based on the following criteria: (1) the proportion of ^{15}N isotope in the heavy component was constrained from 55% to 90% and (2) the R^2 value between the theoretical and experimental intensities in the isotopic envelopes (that primarily result from ~1% natural presence of ^{13}C) for light and heavy components had to be at least 0.9 and 0.5, correspondingly. Deviation of peptide mass derived from the experimental data from the theoretical was limited with 5 ppm (after zero-centering the mass measurement error histogram to account for imperfect mass spectrometer instrument calibration). Peak picking was performed using wavelet-based approach (Du et al., 2006). The signal-to-noise ratio of detected peaks was required to be at least 3.

The proportion of ^{15}N-labeled peptide was log-transformed for convenience of visualization $\log 2\left(\frac{P_{N15}}{P_{N14}+P_{N15}}\right)$, further denoted as x. Half-lives were calculated if the incorporation data of a certain protein was present for at least three time-points. Calculation of the protein half-lives included following steps:

We assumed that, during the three-day pulse labeling, the total protein abundance did not change significantly in the sterile adult worms, whereby protein synthesis equals degradation, collectively designated as protein turnover:

$$P_0 = P_{N14} + P_{N15} \text{ and } \frac{d[P_{N15}]}{dt} + \frac{d[P_{N14}]}{dt} = 0$$

The change in ^{14}N-labeled proteins with time is:

$$\frac{d[P_{N14}]}{dt} = -k_{dp}[P_{N14}]$$

or

$$P_{N14} = P_0 \times e^{-k_{dp} \times \Delta t}$$

In this equation, P_0 is the total protein concentration right before the labeling pulse, k_{dp} is the protein degradation kinetic constant and Δt is pulse length. According to the previous assumption, protein concentration does not change during pulse labeling. Therefore:

$$\frac{P_{N14}}{P_{N14} + P_{N15}} = e^{-k_{dp} \times \Delta t}$$

Plugging-in the proportion of ^{15}N as x and log-transforming the equations results in:

$$\ln(1 - x) = -k_{dp} \times \Delta t$$

Protein half-life could be estimated using following equation:

$$t_{1/2} = \frac{\ln(2)}{k_{dp}}$$

The differences in half-lives between the two strains were tested using the moderated *t*-test (*limma* Bioconductor package) (Ritchie et al., 2015), only when the particular peptide was identified in at least two replicates per strain. The within-group residuals followed a normal distribution as it has been assessed with Q-Q normality plots. The variances within each group were estimated using the *limma* R package. The account for heteroskedasticity was not justified, showing similar variances among groups. *P*s were adjusted for multiple testing according to Benjamini and Hochberg's method (Hochberg and Benjamini, 1990). The SILeNCe pipeline is outlined in Figure 1 and the filtering criteria are summarized in Supplementary Figure 2.

TEM

Transverse sections of three young adults *glp-4(bn2ts)I;daf-2(e1370)III* and *glp-4(bn2ts)I daf-16(mgDf50)I; daf-2(e1370)III*, sampled on the second day of adulthood in a previous study (Depuydt et al., 2013), were reanalyzed using transmission electron microscopy (TEM) to investigate rough endoplasmic reticulum organization. Electron microscopy analysis was done using a Jeol JEM 1010 (Jeol, Tokyo, Japan) operating at 60 kV. Images were digitized using a DITABIS system (Pforzheim, Germany).

Feeding RNAi

Worms were fed RNAi bacteria that were selected from the Ahringer library (Kamath and Ahringer, 2003) and induced as described previously (Timmons et al., 2001).

Lifespan assay

Synchronized L1 worms were placed on NGM plates seeded with RNAi bacteria containing the empty control vector L4440 or a vector expressing *daf-16* dsRNA. Worms were grown at 17°C until the third larval stage (L3) and then switched to 24°C for the remainder of the experiment. Adult lifespan was monitored on a daily basis

and worms were regularly transferred to fresh RNAi plates. Graphpad Prism version 6.05 for Windows (Graphpad Software, La Jolla California, USA) was used for survival analysis and generation of the survival graphs. Median survival was compared using a Log-rank (Mantel Cox) test.

Supplemental References

Du, P., Kibbe, W.A., and Lin, S.M. (2006). Improved peak detection in mass spectrum by incorporating continuous wavelet transform-based pattern matching. Bioinformatics *22*, 2059-2065.

Hochberg, Y., and Benjamini, Y. (1990). More powerful procedures for multiple significance testing. Stat Med *9*, 811-818.

Kamath, R.S., and Ahringer, J. (2003). Genome-wide RNAi screening in Caenorhabditis elegans. Methods *30*, 313-321.

Kessner, D., Chambers, M., Burke, R., Agus, D., and Mallick, P. (2008). ProteoWizard: open source software for rapid proteomics tools development. Bioinformatics *24*, 2534-2536.

Kim, S., and Pevzner, P.A. (2014). MS-GF+ makes progress towards a universal database search tool for proteomics. Nat Commun *5*, 5277.

Lewis, J.A., and Fleming, J.T. (1995). Basic culture methods. Methods in cell biology *48*, 3-29.

Mayampurath, A.M., Jaitly, N., Purvine, S.O., Monroe, M.E., Auberry, K.J., Adkins, J.N., and Smith, R.D. (2008). DeconMSn: a software tool for accurate parent ion monoisotopic mass determination for tandem mass spectra. Bioinformatics *24*, 1021-1023.

Petyuk, V.A., Mayampurath, A.M., Monroe, M.E., Polpitiya, A.D., Purvine, S.O., Anderson, G.A., Camp, D.G., 2nd, and Smith, R.D. (2010a). DtaRefinery, a software tool for elimination of systematic errors from parent ion mass measurements in tandem mass spectra data sets. Mol Cell Proteomics *9*, 486-496.

Petyuk, V.A., Qian, W.J., Smith, R.D., and Smith, D.J. (2010b). Mapping protein abundance patterns in the brain using voxelation combined with liquid chromatography and mass spectrometry. Methods *50*, 77-84.

Ritchie, M.E., Phipson, B., Wu, D., Hu, Y., Law, C.W., Shi, W., and Smyth, G.K. (2015). limma powers differential expression analyses for RNA-sequencing and microarray studies. Nucleic Acids Res *43*, e47.

Timmons, L., Court, D.L., and Fire, A. (2001). Ingestion of bacterially expressed dsRNAs can produce specific and potent genetic interference in Caenorhabditis elegans. Gene *263*, 103-112.